INORGANIC CHEMISTRY FRONTIERS

REVIEW

View Article Online
View Journal | View Issue

Cite this: *Inorg. Chem. Front.*, 2024, **11**, 7756

Research progress in optical materials with cationic organic planar π-conjugated groups containing C═N bonds

Hangwei Jia,[a] Xueling Hou *[a,b] and Shilie Pan *[a,b]

Recently, organic planar π-conjugated groups have received increasing attention from researchers for the construction of linear/nonlinear optical crystals with excellent performance in the UV/DUV region. Compared with inorganic optically active units ($[BO_3]^{3-}$, $[B_3O_6]^{3-}$, $[CO_3]^{2-}$, and $[NO_3]^-$), organic planar π-conjugated groups have larger microscopic hyperpolarizability and polarizability anisotropy, which enable the synthesis of birefringent crystals with large birefringence or NLO crystals with a high SHG response and large birefringence. Among the various types of organic planar π-conjugated groups, cationic organic planar π-conjugated groups containing C═N bonds show several great advantages, including high nonlinear polarizability, high flexibility in molecular design and assembly and easy large-size crystal growth. These merits have inspired researchers to make great efforts to develop high-performance optical crystals for application in the UV/DUV region. In this review, the compounds containing cationic organic planar π-conjugated groups (such as $[C_3N_6H_7]^+$, $[C(NH_2)_3]^+$, $[C_5NH_6O]^+$, $[C_4N_3H_6]^+$, *etc.*) are outlined. The relationship between the optical properties and the structure is discussed in accordance with the available computational and experimental data. The above types of compounds are summarised and evaluated. Finally, the main challenges and future opportunities for the construction of optical crystals using cationic organic planar π-conjugated groups are presented, and the prospects for development are outlooked.

Received 3rd September 2024,
Accepted 26th September 2024

DOI: 10.1039/d4qi02232g

rsc.li/frontiers-inorganic

10th anniversary statement

I'm Shilie Pan. It's my pleasure to participate in the celebration of the "10th anniversary of *Inorganic Chemistry Frontiers*". My current research interests include the design, synthesis, crystal growth and evaluation of novel optoelectronic functional materials. My first article entitled "$Ba_{n+2}Zn_n(BO_3)_n(B_2O_5)F_n$ (n = 1, 2): new members of the zincoborate fluoride series with two kinds of isolated B–O units" was accepted in this journal in 2016. Since then, we have published articles in this journal almost every year. These articles have important reference value for the design and development of short-wavelength photoelectric functional materials worldwide. The journal *Inorganic Chemistry Frontiers* actively incorporates advanced scientific research in the field of global inorganic chemistry and its interdisciplinary fields, aiming to establish an excellent platform for international academic communication. It not only promotes research in the field of inorganic chemistry, but also plays an important role in the development of the international chemical community.

1. Introduction

Lasers are widely used in laser lithography, communications, medicine and scanning due to their high brightness, good monochromaticity and excellent coherence.[1–6] Generally speaking, short wavelength lasers have high photon energy, strong penetration and excellent focusing performance. All-solid-state lasers have significant advantages in outputting short-wavelength lasers. Nonlinear optical crystals (especially second harmonic generation (SHG) crystals) and birefringent crystals are the crucial working parts of the all-solid-state laser. Nonlinear optical crystals exhibit second-order nonlinear optical effects and crystallize in the non-central symmetry (NCS) space group, which can be used to adjust the frequency of the laser in order to broaden the tuneable range of the laser.[7,8] Birefringent crystals are widely used as an important part of optical devices such as beam splitters, isolators and optical polarizers due to

[a]*Research Center for Crystal Materials; State Key Laboratory of Functional Materials and Devices for Special Environmental Conditions; Xinjiang Key Laboratory of Functional Crystal Materials; Xinjiang Technical Institute of Physics and Chemistry, Chinese Academy of Sciences, 40-1 South Beijing Road, Urumqi 830011, China. E-mail: xlhou@ms.xjb.ac.cn, slpan@ms.xjb.ac.cn*
[b]*Center of Materials Science and Optoelectronics Engineering, University of Chinese Academy of Sciences, Beijing 100049, China*

their unique birefringent phenomenon.[9–11] As laser-optical technology continues to develop, there is an urgent need to develop nonlinear optical crystals and birefringent crystals with superior performance to meet the increasing demand for lasers.

After decades of research by crystallographic researchers, numerous nonlinear optical and birefringent crystals with outstanding properties have been developed, such as the nonlinear optical crystals $KTiOPO_4$ (KTP), β-BaB_2O_4 (BBO), LiB_3O_5 (LBO), $CsLiB_6O_{10}$ and $KBe_2BO_3F_2$ (KBBF), and the commercial birefringent crystals MgF_2, α-BaB_2O_4, $CaCO_3$, and others.[12–21] The microstructure of the crystals is closely related to the macroscopic optical properties. Conformational studies of crystals reveal the important role of microscopic optically active units in the manifestation of optical properties of nonlinear optical crystals and birefringent crystals.[22–24] Nonlinear optical coefficients, birefringence and UV cutoff edge are important optical parameters of nonlinear optical crystals.[7] Important parameters of ultraviolet (UV) birefringent crystals are birefringence and UV cutoff edge. The large birefringence is favourable for the miniaturization of optical devices.[25] According to the anionic group theory, the anionic groups of the crystal structure are the main determinants of its macroscopic optical properties.[26,27] For the nonlinear optical crystals, the macroscopic SHG coefficient is the geometric superposition of the microscopic SHG coefficient of the anion group, that is, the nonlinear optical coefficient of the crystal is dependent on the type of microscopic optically active unit and its arrangement in the crystal structure.[26] For birefringent crystals, the birefringence of the crystal is determined by its own optical anisotropy, depending on the polarizability anisotropy of the microscopic optically active units and their arrangement in the crystal lattice.[28,29] Anionic groups can be categorized into π-conjugated and non-π-conjugated groups according to the type of chemical bond. In general, the main non-π-conjugated groups are $[BO_xF_{4-x}]^{x-5}$ (x = 0–4), $[PO_4]^{3-}$, $[PO_3F]^{2-}$, $[PO_2F_2]^{-}$, $[SO_4]^{2-}$, $[SO_3F]^{-}$, and $[SiO_4]^{4-}$.[10,30–39] The main π-conjugated units are $[BO_3]^{3-}$, $[B_3O_6]^{3-}$, $[CO_3]^{2-}$, $[NO_3]^{-}$, $[H_xC_3N_3O_3]^{x-3}$ (x = 0–3) and $[H_xC_4N_2O_3]^{x-4}$ (x = 2, 3).[40–49] In addition, the introduction of halogen anions and metal cations containing non-bonding lone-pair electrons (Pb^{2+}, Sb^{3+}, Bi^{3+}, and Sn^{2+}) into the lattice results in the formation of distorted polyhedra, which has the opportunity to induce the formation of NCS structures.[28,50,51]

In recent years, in addition to the traditional anionic π-conjugated units, some organic planar π-conjugated cations have also gained the attention of researchers due to their excellent optical activity.[24] A series of semi-organic optical crystals with excellent properties have been prepared by combining organic cations with inorganic anions.[49] Compared with traditional inorganic crystals, semi-organic optical crystals have the following unique advantages:[52] (1) the nonlinear polarizability of organic π-conjugated molecules is 1–2 orders higher than that of inorganic crystals; (2) fast response speed; (3) the high laser damage threshold; and (4) great flexibility in molecular design and assembly.

Melamine ($C_3N_6H_6$), a triazine-containing heterocyclic organic compound, is an excellent optically active unit. It has a large π-conjugated geometry similar to $[C_3N_3O_3]^{3-}$ and $[B_3O_6]^{3-}$, which results in a large anisotropy of micro-polarizability. The presence of the N atom within the ring and the NH_2 on the outside of the ring has a tendency to form hydrogen bonds, which is not only favourable for the formation of a coplanar arrangement of melamine, but also for the growth of large size crystals. The interatomic distance of the melamine ring is shorter than that of β-BBO, which implies a large overlap between the C 2p and N 2p orbitals, leading to more strong Pπ–Pπ interactions in the melamine groups.[53] In 2021, Lin's group reported the synthesis of two compounds utilising melamine, $2(C_3H_7N_6)^{+}\cdot 2Cl^{-}\cdot H_2O$ and $(H_7C_3N_6)(H_6C_3N_6)ZnCl_3$, with birefringence values of 0.277@546 nm and 0.26@1064 nm, respectively.[53,54] This was the first report on the utilization of $[C_3N_6H_7]^{+}$ groups to construct large birefringence optical crystals. Pan's group synthesized $(C_3N_6H_7)_2(B_3O_3F_4(OH))$ by using the π-conjugated unit binding strategy. It currently has the largest birefringence (0.44@546 nm) of melamine-based compounds in the UV region.[55] $(C_3N_6H_8)PbBr_4$ was reported by the Zhao's group, which exhibits a large birefringence (0.294@550 nm).[56] The melamine groups $[C_3N_6H_{6+x}]^{x+}$ (x = 0–2) demonstrate significant polarizability anisotropy in these compounds, which can produce large birefringence when properly arranged. In addition, the planar π-conjugated $[C_5N_2H_7]^{+}$, $[C_5NOH_{5+x}]^{x+}$ (x = 0–1), $[C_4N_3H_6]^{+}$, $[C_4N_3OH_6]^{+}$, and $[C_3N_2H_5]^{+}$ groups are considered to have high optical activity for the construction of large birefringent crystals.[57–61] The $[C(NH_2)_3]^{+}$ organic cation has a planar triangular geometrical configuration similar to $[BO_3]^{3-}$ and possesses more π electrons, which will have a beneficial influence on the nonlinear optical coefficients and birefringence; similar to melamine, the NH_2 units in the $[C(NH_2)_3]^{+}$ groups are also inclined to generate hydrogen bonding, which is favourable for the $[C(NH_2)_3]^{+}$ groups to form a coplanar arrangement and enhance the nonlinear optical effect and birefringence, and facilitate crystal growth; the terminal hydrogen of the N atom eliminates the dangling bonds of the terminal N atom, favouring the UV cutoff edge blueshift.[62–65] In 2017, Becker investigated the nonlinear optical properties of guanidinium phosphate, confirming the guanidinium group to be an excellent optically active unit.[66]

Some compounds containing organic planar cations have been reported in some reviews, but they have not been systematically summarized and reported. In this review, we classified and summarized emerging compounds containing organic planar π-conjugated cations (including $[C_3N_6H_{6+x}]^{x+}$ (x = 0–2), $[C(NH_2)_3]^{+}$, $[C_5N_2H_7]^{+}$, $[C_5NOH_{5+x}]^{x+}$ (x = 0–1), $[C_4N_3H_6]^{+}$, $[C_4N_3OH_6]^{+}$, and $[C_3N_2H_5]^{+}$). The polarizability anisotropy, hyperpolarizability and HOMO–LUMO gap of organic cations are calculated using the DFT method implemented using the Gaussian09 package at the B3LYP/6-31G level (Fig. 1). Based

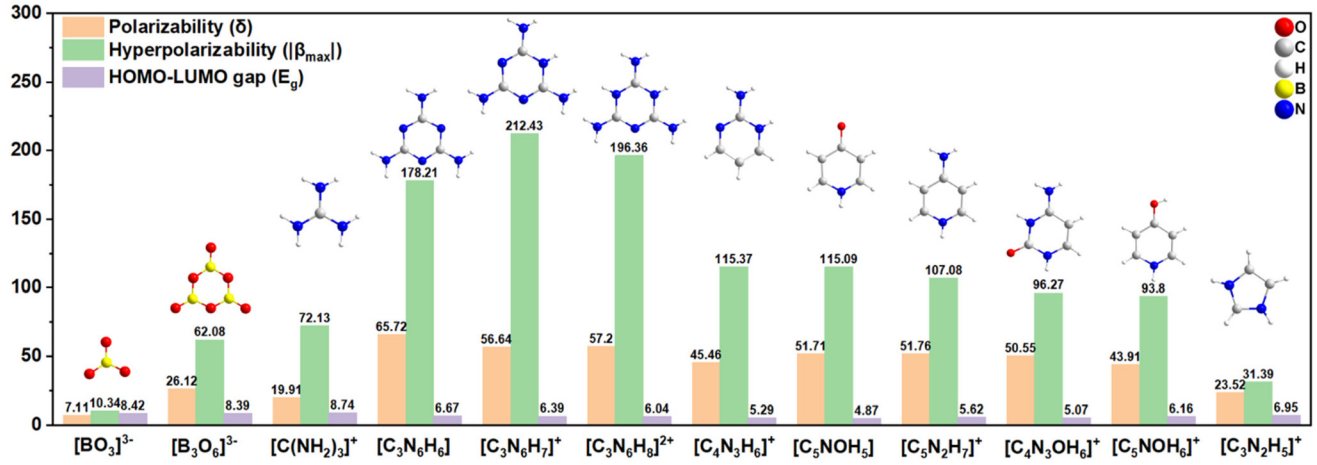

Fig. 1 The calculated polarizability anisotropy, hyperpolarizability and HOMO–LUMO gap of the optically active groups.

on the available experimental and computational data, the crystal structure and main optical properties of these compounds are discussed in detail. The influences of different anions on the arrangement of organic cations are explored. The prospect of the design of the compounds containing organic cationic groups is presented in order to provide some valuable references for the research of optical crystals containing organic cationic compounds.

2. Optical crystals containing planar π-conjugated organic cations

In this section, compounds containing organic planar π-conjugated cations are mainly involved with $[C_3N_6H_{6+x}]^{x+}$ (x = 0–2), $[C(NH_2)_3]^+$, $[C_5N_2H_7]^+$, $[C_5NOH_{5+x}]^{x+}$ (x = 0–1), $[C_4N_3H_6]^+$, $[C_4N_3OH_6]^+$, and $[C_3N_2H_5]^+$ groups. These compounds are classified and summarized. The relationship between the crystal structure and linear/nonlinear optical properties of the above crystals is also discussed in detail from the perspective of nonlinear/birefringent optically active units.

2.1 Optical crystal with $[C_3N_6H_{6+x}]^{x+}$ (x = 0–2) groups

In this section, nonlinear optical crystals and birefringent crystals containing $[C_3N_6H_{6+x}]^{x+}$ (x = 0–2) groups are mainly discussed. Such crystals not only exhibit a suitable band gap, but also have a large birefringence. The optical properties of the crystals are shown in Table 1.

$2(C_3H_7N_6)^+\cdot 2Cl^-\cdot H_2O$ belongs to the NCS orthorhombic space group $Cmc2_1$.[53] The asymmetric unit of 2 $(C_3H_7N_6)^+\cdot 2Cl^-\cdot H_2O$ contains two chloride ions, one water, and one $[C_3N_6H_7]^+$ group. As shown in Fig. 2, the $[C_3N_6H_7]^+$ rings

Table 1 Main optical properties of the compounds containing the $[C_3N_6H_{6+x}]^{x+}$ (x = 0–2) groups

Number	Compound	Space group	Band gap[a] (eV)	Density ($\times 10^{-3}$ Å^{-3})	Birefringence[b] (@546 nm)	UV cut-off (nm)	SHG response[a]	Ref.
1	$(C_3N_6H_8)PbBr_4$	$P2_1/c$	3.13	3.14	0.294@550 nm	374	—	56
2	$(C_3N_6H_8)SnCl_4$	$Pna2_1$	3.71	3.45	0.34@550 nm	334	—	70
3	$(H_7C_3N_6)\cdot(H_6C_3N_6)ZnCl_3$	$P2_1$	3.95[b]	5.35	0.26@1064 nm	236	2.8 × KDP	54
4	$(C_3N_6H_6)_4HPF_6$	$R\bar{3}c$	4.12	4.57	0.264	300	—	71
5	$(C_3N_6H_7)_3HgCl_5$	$P\bar{1}$	4.19	3.38	0.093@1064 nm	290	—	72
6	$(C_3N_6H_6)_2(C_3N_6H_7)PF_6\cdot H_2O$	$P2_1/c$	4.20	5.77	0.243	300	—	71
7	$(C_3N_6H_7)\cdot(C_3N_6H_6)HgCl_3$	$P2_1$	4.40	5.23	0.246@1064 nm	278	5 × KDP	72
8	$H_6C_3N_6$	$P2_1/c$	4.60	7.73	0.26	248	—	67 and 68
9	$(C_3H_7N_6)_6(H_2PO_4)_4(HPO_4)\cdot 4H_2O$	$P2_1$	4.6	—	0.22@1064 nm	—	0.1 × KDP	73
10	$(C_3H_7N_6)_2SO_4\cdot 2H_2O$	$P\bar{1}$	4.62	5.25	—	—	—	73
11	$(C_3H_7N_6)_2Cl_2\cdot H_2O$	$C2/m$	4.70	5.63	0.33@550 nm	230	—	67
12	$(C_3H_7N_6)F\cdot H_2O$	$C2/m$	4.72	6.00	0.38@550 nm	220	—	67
13	$(C_3N_6H_7)_2(B_3O_3F_4(OH))$	$P\bar{1}$	4.72	4.98	0.44	240	—	55
14	$(C_3N_6H_7)_2SbF_5\cdot H_2O$	$P\bar{1}$	4.74	4.89	0.38@550 nm	220	—	74
15	$2(C_3H_7N_6)^+\cdot 2Cl^-\cdot H_2O$	$Cmc2_1$	4.75	5.58	0.277	245	4.3 × KDP	53
16	$(C_3N_6H_7)_2SiF_6\cdot H_2O$	$P2_1/c$	4.76	5.31	0.152@550 nm	220	—	75
17	$(C_3N_6H_7)SO_3CH_3\cdot H_2O$	$P\bar{1}$	4.80	3.94	0.31	233	—	69
18	$(C_3N_6H_7)BF_4\cdot H_2O$	$P\bar{1}$	5.05	3.39	0.37	244	—	69
19	$C_3N_6H_7SO_3NH_2$	$P\bar{1}$	5.53	3.20	0.34	206	—	68

[a] The experimental value. [b] The theoretical calculation value.

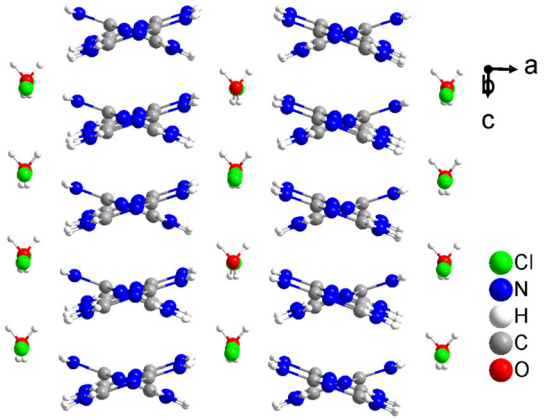

Fig. 2 Crystal structure of $2(C_3H_7N_6)^+ \cdot 2Cl^- \cdot H_2O$.

are interconnected through N–H···N hydrogen bonds, forming chains along the *b*-axis. These chains are further linked by N–H···Cl hydrogen bonds. In the meantime, the rings of $[C_3N_6H_7]^+$ are arranged in a π–π stacked formation along the *c*-direction to form a stereo configuration. $2(C_3H_7N_6)^+ \cdot 2Cl^- \cdot H_2O$ exhibits a large birefringence (Δn = 0.277@546 nm), a short UV cutoff edge (245 nm) and a high SHG response (4.3 × KDP). Theoretical calculations and structural analyses show that the optical properties of $2(C_3H_7N_6)^+ \cdot 2Cl^- \cdot H_2O$ are primarily ascribed to the planar π-conjugated $[C_3N_6H_7]^+$ groups. The $[C_3N_6H_7]^+$ groups are ideal active groups for UV nonlinear optical materials, which will offer fresh insights for discovering innovative UV nonlinear optical and birefringent materials.

Both β-$(C_3H_7N_6)_2Cl_2 \cdot H_2O$ and $(C_3H_7N_6)F \cdot H_2O$ crystallize in the same monoclinic space group $C2/m$.[67] They exhibit comparable structural characteristics (Fig. 3 and 4). The asymmetric unit of β-$(C_3H_7N_6)_2Cl_2 \cdot H_2O$ consists of two chlorine atoms, one water, and two $[C_3N_6H_7]^+$ groups. In the *ab*-plane, adjacent $[C_3N_6H_7]^+$ groups are connected by hydrogen bonding between NH_2 and N atoms to form a chain along the *a*-axis. The chains are further connected by N–H···Cl and N–H···O hydrogen bonds to build a two-dimensional planar structure. Meanwhile, the $[C_3N_6H_7]^+$ groups are stacked along the *c*-axis by π–π interactions. The almost perfectly parallel arrangement of the $[C_3N_6H_7]^+$ groups contributes positively to the macroscopic optical anisotropy of the crystals. The N–H···F hydrogen bonding in $(C_3H_7N_6)F \cdot H_2O$ results in closer stacking of the $[C_3N_6H_7]^+$ groups along the *c*-axis than in the $(C_3H_7N_6)_2Cl_2 \cdot H_2O$ structures. The density of the $[C_3N_6H_7]^+$ groups in $(C_3H_7N_6)F \cdot H_2O$ is greater than that in $(C_3H_7N_6)_2Cl_2 \cdot H_2O$, which results in higher polarization anisotropy. The band gaps of β-$(C_3H_7N_6)_2Cl_2 \cdot H_2O$ and $(C_3H_7N_6)F \cdot H_2O$ are 4.70 and 4.72 eV, the UV cutoff edges are 230 and 220 nm, and the birefringence values are 0.33 and 0.38@550 nm, respectively. The difference in optical properties between β-$(C_3H_7N_6)_2Cl_2 \cdot H_2O$ and $(C_3H_7N_6)F \cdot H_2O$ is attributed to the density of the $[C_3N_6H_7]^+$ groups in the crystal structure. The parallel arrangement of the $[C_3N_6H_7]^+$ groups can be explained by N–H···X (X = Cl and F) hydrogen bond interactions. The introduction of halogen atoms facilitates the uniform orientation of the planar $[C_3N_6H_7]^+$ groups. This strategy is beneficial for the construction of birefringent materials with excellent properties.

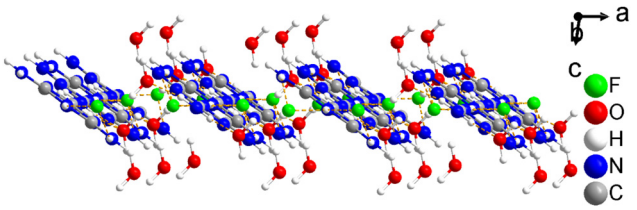

Fig. 4 Crystal structure of $(C_3H_7N_6)F \cdot H_2O$.

$C_3H_8N_6I_6 \cdot 3H_2O$ belongs to the monoclinic space group $P2_1$.[25] As shown in Fig. 5, the crystal structure of $C_3H_8N_6I_6 \cdot 3H_2O$ consists of the melamine organic cation $[C_3H_8N_6]^{2+}$ groups and the inorganic linear $[I_3]^-$ anion. The $[I_3]^-$ anion aligns along the *a*-axis, forming an infinitely long linear chain with a distance of about 3.65 Å between $[I_3]^- \cdots [I_3]^-$, which is significantly larger than the distance between I–I in the linear $[I_3]^-$ chain (2.8583(8) to 3.0764(8) Å). The adjacent $[C_3H_8N_6]^{2+}$ groups form hydrogen bonds with water molecules, which are evenly distributed in the polyiodide infinite

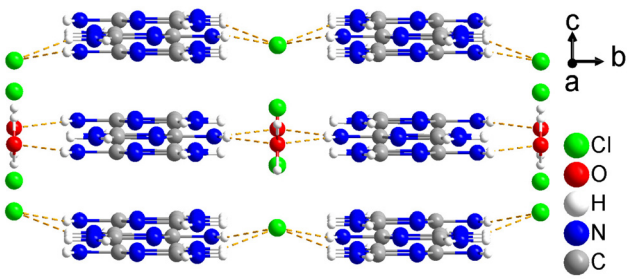

Fig. 3 Crystal structure of β-$(C_3H_7N_6)_2Cl_2 \cdot H_2O$.

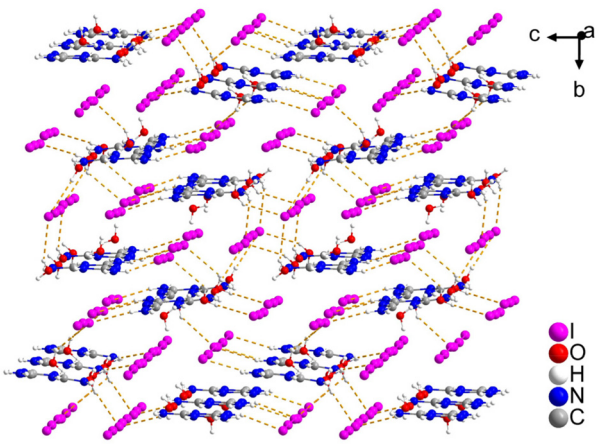

Fig. 5 Crystal structure of $C_3H_8N_6I_6 \cdot 3H_2O$.

chain. The hydrogen bonds between $[C_3H_8N_6]^{2+}$ groups and $[I_3]^-$ units play a crucial role in stabilizing the crystal structure. Black crystals of $C_3H_8N_6I_6{\cdot}3H_2O$ with a size up to 13 × 4 × 2 mm^3 were successfully grown using the solution cooling method. It is particularly noteworthy that the birefringence of the $C_3H_8N_6I_6{\cdot}3H_2O$ crystal is as high as 2.8 in the visible to infrared spectral range, which is about 3.7 times higher than that of the record-holder $BaTiS_3$. Through critical point analysis and first-principles calculations, it has been determined that the parallel arrangement of the linear $[I_3]^-$ units is primarily responsible for the significant optical anisotropy, which causes the largest difference in polarizabilities along different crystallographic axes. This study demonstrates the great potential of polyiodide crystals for the development of miniaturized and highly efficient polarization optical devices.

$C_3N_6H_7SO_3NH_2$ crystallizes in the space group $P\bar{1}$.[68] As shown in Fig. 6, the basic structural units are planar $[C_3N_6H_7]^+$ groups and tetrahedral $[NH_2SO_3]^-$ units. In particular, the $[C_3N_6H_7]^+$ groups are connected by hydrogen bonds to form a one-dimensional chain in the *bc* plane. Multiple parallel chains of $[C_3N_6H_7]^+$ are connected by hydrogen bonds from the $[NH_2SO_3]^-$ units, extending indefinitely along the *a* direction to form a two-dimensional plane. The parallel arrangement of the π-conjugated $[C_3N_6H_7]^+$ groups results in an efficient organization of π electrons, which enhances the optical anisotropy of the structure. The planar layers are connected by hydrogen bonds to form a three-dimensional network structure in the *c* direction. The $[C_3N_6H_7]^+$ groups and $[NH_2SO_3]^-$ units in the adjacent layers are arranged in an inverted parallel manner, forming a centrosymmetric structure. The band gap of $C_3N_6H_7SO_3NH_2$ is 5.53 eV, the UV cutoff edge is 206 nm, and the calculated birefringence is 0.34@546 nm. Theoretical calculations show that the excellent optical properties of $C_3N_6H_7SO_3NH_2$ are contributed by the synergistic interaction between the planar π-conjugated $[C_3N_6H_7]^+$ groups and tetrahedral $[NH_2SO_3]^-$ units.

$(C_3N_6H_7)BF_4{\cdot}H_2O$ crystallizes in the space group $P\bar{1}$.[69] The basic structural unit of $(C_3N_6H_7)BF_4{\cdot}H_2O$ consists of planar $[C_3N_6H_7]^+$ groups, tetrahedral $[BF_4]^-$ units and water molecules (Fig. 7a). The long chains of $[C_3N_6H_7]^+$ groups are interconnected by hydrogen bonds. Multiple parallel chains of $[C_3N_6H_7]^+$ extend indefinitely in the layer, forming a two-dimensional plane. The layers are linked through hydrogen bonds to form a network structure. As depicted in Fig. 7b, the transparent crystals of $(C_3N_6H_7)BF_4{\cdot}H_2O$ with a size up to 24 × 4 × 0.17 mm^3 were grown using the solution cooling method. The growth habit of the crystal was characterised by two-dimensional extension. The band gap of $(C_3N_6H_7)BF_4{\cdot}H_2O$ is 5.05 eV, the UV cutoff edge is 244 nm, and the birefringence is 0.37@546 nm. These works show that organic–inorganic hybrid crystals with planar π-conjugated groups and non-π-conjugated tetrahedral units are promising systems for UV optical materials.

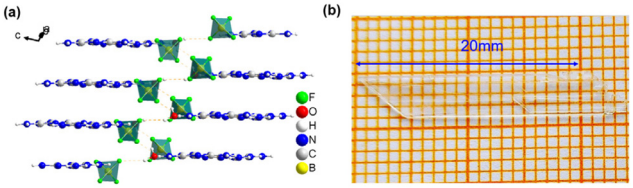

Fig. 7 (a) Crystal structure of $(C_3N_6H_7)BF_4{\cdot}H_2O$. (b) The as-grown crystal of $(C_3N_6H_7)BF_4{\cdot}H_2O$. Copyright 2024 Royal Society of Chemistry.

$(H_7C_3N_6)(H_6C_3N_6)ZnCl_3$ crystallizes in the NCS space group $P2_1$.[54] The nitrogen atom from the melamine ring and three chlorine atoms together form a distorted $[ZnNCl_3]$ polyhedron. The adjacent $[ZnNCl_3]$ polyhedron arranged along the *c* direction is positioned in the opposite direction (Fig. 8). All the $[H_7C_3N_6]^+$ and $[H_6C_3N_6]$ groups are arranged parallelly along the *b*-axis, which has a positive influence on NLO susceptibilities. The adjacent melamine rings are connected by hydrogen bonds to form a chain along the *c*-axis. The 2D structure is formed between the chains by N–H···Cl hydrogen bonds. $(H_7C_3N_6)(H_6C_3N_6)ZnCl_3$ exhibits a strong SHG response (2.8 × KDP), a large birefringence (Δn = 0.26@1064 nm) and a short cutoff edge (236 nm). Theoretical calculations show that the optical properties are mainly contributed by the $[C_3N_6]$ ring and distorted $[ZnNCl_3]$ polyhedron.

$(C_3N_6H_7)(C_3N_6H_6)HgCl_3$ crystallizes in the NCS group $P2_1$.[72] As shown in Fig. 9, the $[HgCl_3]^-$ unit is linked to the internal N atom of melamine to form a large asymmetric $[C_3N_6H_6HgCl_3]^-$ group, which rotates along the *b*-axis to form pseudo helical chains. These chains are further aligned in the *bc* plane to produce a pseudo two-dimensional structure. The layers are stacked along the *a*-axis to form a 3D structure. The $[C_3N_6H_7]^+$

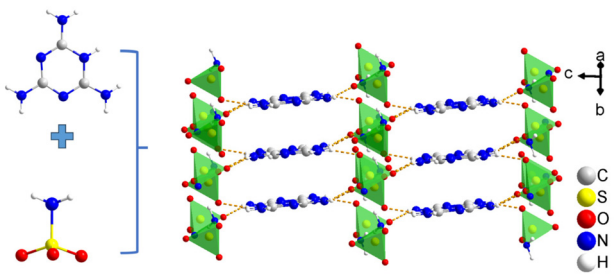

Fig. 6 Crystal structure of $C_3N_6H_7SO_3NH_2$.

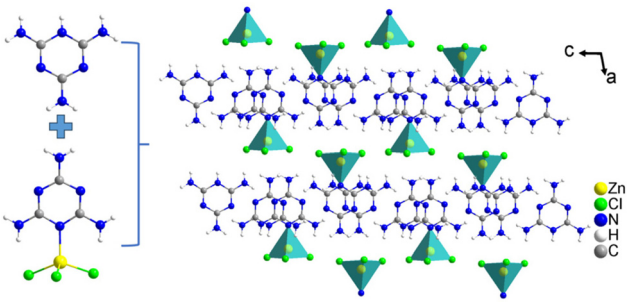

Fig. 8 Crystal structure of $(H_7C_3N_6)(H_6C_3N_6)ZnCl_3$.

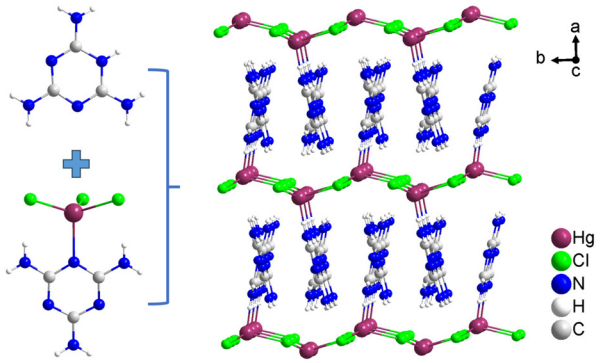

Fig. 9 Crystal structure of $(C_3N_6H_7)(C_3N_6H_6)HgCl_3$.

cations fill the interlayer to maintain the charge balance. The NCS structure of $(C_3N_6H_7)(C_3N_6H_6)HgCl_3$ is determined by two distinct properties: the large asymmetric $[C_3N_6H_6HgCl_3]^-$ groups formed by the direct covalent coordination of melamine and Hg^{2+} result in localized noncentrality of inorganic modules; the small dihedral angle among the melamine rings prevents the harmful anti-parallel arrangement of the planar organic groups. $(C_3N_6H_7)(C_3N_6H_6)HgCl_3$ exhibits a band gap of 4.40 eV, a UV cut-off edge of 278 nm, and a birefringence of 0.246@1064 nm. More importantly, $(C_3N_6H_7)(C_3N_6H_6)HgCl_3$ exhibits a strong SHG response (5 × KDP). The theoretical calculation shows that the π-conjugated system of melamine and the Hg^{2+} heavy metal cation has large polarizability, making a major contribution to the nonlinear optics of the crystal, while the optical anisotropy is mainly dominated by the organic groups.

$(C_3N_6H_8)SnCl_4$ belongs to the NCS space group $Pna2_1$.[70] The structural unit consists of $[C_3N_6H_8]^{2+}$ cation groups and $SnCl_4$ tetrahedra (Fig. 10). The $[C_3N_6H_8]^{2+}$ groups in the crystal structure of $(C_3N_6H_8)SnCl_4$ are arranged parallelly. The dihedral angle of the adjacent $[C_3N_6H_8]^{2+}$ plane in the crystal structure is about 61°, and the Sn atom is coordinated with four chlorine atoms to form a highly distorted $[SnCl_4]^{2-}$ seesaw. The $[SnCl_4]^{2-}$ seesaws are also nonparallel. The adjacent $[SnCl_4]^{2-}$ groups are almost perpendicular to each other. The Sn^{2+} ion in $[SnCl_4]^{2-}$ interacts with the Cl atom from the adjacent $[SnCl_4]^{2-}$ tetrahedron to form four additional Sn–Cl bonds, which form an infinitely scalable 2D pseudo-perovskite layer. The layers are filled with melamine cations and connected to the inorganic layers by N–H···Cl hydrogen bonds. The analysis shows that the arrangement of planar melamine cations and distorted $[SnCl_4]^{2-}$ tetrahedra in the structure has an adverse effect on the high optical anisotropy of the crystal. The band gap of $(C_3N_6H_8)SnCl_4$ is 3.71 eV, the UV cutoff edge is 334 nm and the calculated birefringence is 0.34@550 nm. Theoretical calculations show that birefringence is contributed by $[C_3N_6H_8]^{2+}$ groups and the Sn^{2+} cation of the highly distorted $[SnCl_4]^{2-}$ tetrahedron. However, the arrangement of $[C_3N_6H_8]^{2+}$ groups and the distorted $[SnCl_4]^{2-}$ tetrahedron could not achieve the optimal structural anisotropy. Therefore, additional research on hybrid halide perovskite materials is needed to synthesize birefringent crystals with excellent properties.

$(C_3N_6H_8)PbBr_4$ crystallizes in the centrosymmetric monoclinic space group $P2_1/c$.[56] As shown in Fig. 11, the crystal structure of $(C_3N_6H_8)PbBr_4$ consists of a $PbBr_6$ octahedron and $[C_3N_6H_8]^{2+}$ groups. It is considered to be a (110) oriented perovskite skeleton composed of corrugated layers, with the $[C_3N_6H_8]^{2+}$ cation connected to the $[PbBr_4]_\infty$ layer by weak N–H···Br hydrogen bonds. The band gap of $(C_3N_6H_8)PbBr_4$ is about 3.13 eV, corresponding to a UV cutoff edge of 374 nm. The calculated birefringence is 0.294@550 nm, which is the highest among reported halide perovskite materials. First principles calculations show that melamine π-conjugated groups and highly distorted $PbBr_6$ octahedra are the main contributing factors to the birefringence of $(C_3N_6H_8)PbBr_4$. However, the $[C_3N_6H_8]^{2+}$ cation and $PbBr_6$ octahedron are not parallel in the crystal structure, and Pb^{2+} lone pair electrons are inert in stereochemistry; the birefringence of hybrid halide perovskites still has great space for improvement.

$[C_3N_6H_7]_2[B_3O_3F_4(OH)]$ crystallizes in the triclinic space group $P\bar{1}$.[55] As shown in Fig. 12, $[B_3O_3F_4(OH)]^{2-}$ groups consist of $[BO_2F_2]^{2-}$ and $[BO_2(OH)]^{2-}$ units, and the $[B_3O_3F_4(OH)]^{2-}$ groups appear in pairs through O–H···O interactions. Similarly, the $[C_3N_6H_7]^+$ rings are paired by N–H···N hydrogen bonds. $[B_3O_3F_4(OH)]^{2-}$ and $[C_3N_6H_7]^+$ groups form one-dimensional chains under the action of hydrogen bonds. The chains are connected by hydrogen bonds and extend on the plane to

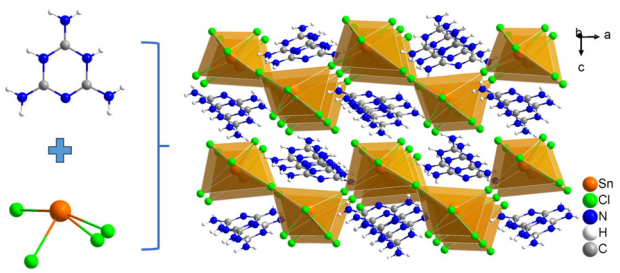

Fig. 10 Crystal structure of $(C_3N_6H_8)SnCl_4$.

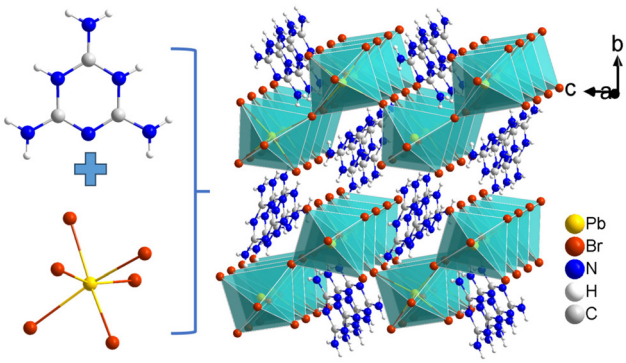

Fig. 11 Crystal structure of $(C_3N_6H_8)PbBr_4$.

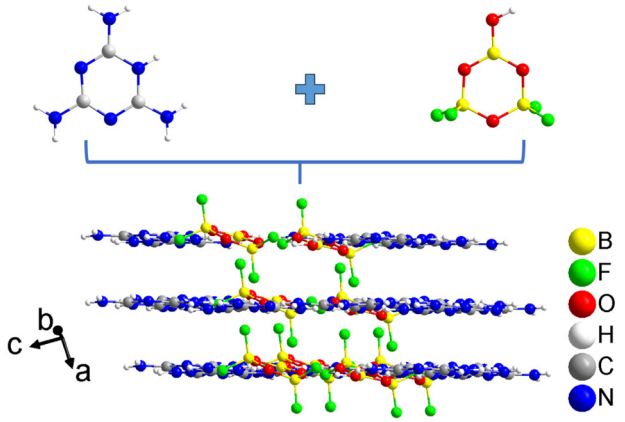

Fig. 12 Crystal structure of $[C_3N_6H_7]_2[B_3O_3F_4(OH)]$.

form two-dimensional layer structures. $[C_3N_6H_7]_2[B_3O_3F_4(OH)]$ exhibits a relatively short UV cutoff edge of 240 nm and a birefringence of 0.440@546 nm. The real-space atomic cutting and response electron distribution anisotropy (REDA) analysis show that the large birefringence is mainly contributed by the $[B_3O_3F_4(OH)]^{2-}$ and $[C_3N_6H_7]^+$ groups. This strategy may provide a new way to explore UV birefringent crystals in semi-organic systems.

The birefringence of optical materials primarily depends on the density of birefringent active groups and their arrangement within the crystal structure. The $[C_3N_6H_7]^+$ group has a large π-conjugated geometry, which shows excellent optical anisotropy. In accordance with the "π-conjugated confinement" principle reported by Chen's group,[30] the introduction of non-π-conjugated units into the π-conjugated system can limit the density of π-conjugated groups and expand the band gap. The effect of different anions on the density and arrangement of $[C_3N_6H_7]^+$ groups, as well as the influence of the density and arrangement of $[C_3N_6H_7]^+$ groups on the birefringence of the crystal have been discussed in detail. As shown in Table 1, for compounds consisting only of π-conjugated groups, such as $C_3N_6H_7$, $2(C_3N_6H_7)^+\cdot 2Cl^-\cdot H_2O$, $(C_3N_6H_7)_2Cl_2\cdot H_2O$ and $(C_3N_6H_7)F\cdot H_2O$, their $[C_3N_6H_7]^+$ density is 7.73, 5.58, 5.63 and 6.00 × 10^{-3} Å^{-3}, respectively. The density of $[C_3N_6H_7]^+$ can be effectively reduced by introducing a non-π-conjugate polyhedron into crystal structures. For crystals such as $(C_3N_6H_7)_3HgCl_5$, $(C_3N_6H_7)_2SiF_6\cdot H_2O$, $(H_7C_3N_6)\cdot(H_6C_3N_6)ZnCl_3$, $(C_3N_6H_6)_4HPF_6$, $(C_3N_6H_7)SO_3NH_2$, $(C_3N_6H_7)BF_4\cdot H_2O$ and $(C_3N_6H_7)SO_3CH_3\cdot H_2O$, their $[C_3N_6H_7]^+$ densities reduced to 3.38, 5.31, 5.35, 4.57, 3.20, 3.39 and 3.94 × 10^{-3} Å^{-3}, respectively. The introduction of non-π-conjugated groups into the crystal structure effectively restricts the density of π-conjugated units. This indicates a significant impact on the overall structure and optical properties of the material. In terms of the band gap of compounds, the introduction of non-π-conjugated tetrahedron units is beneficial for increasing the band gap of compounds, such as $(C_3N_6H_7)SO_3NH_2$, $(C_3N_6H_7)BF_4\cdot H_2O$ and $(C_3N_6H_7)SO_3CH_3\cdot H_2O$, and their band gaps are 5.53, 5.05 and 4.80 eV, respectively.[68,69] However, the introduction of d^0, d^{10} and transition metals such as Hg, Pb, Zn and Sn will reduce the band gap of the compound. Concerning the birefringence of compounds, when $[C_3N_6H_7]^+$ groups are arranged uniformly and parallelly, the crystals have a large birefringence. Exception for the $(C_3N_6H_7)_3HgCl_5$ crystal, where the $[C_3N_6H_7]^+$ groups are also in a parallel arrangement, the birefringence is only 0.093@1064 nm. This is mainly due to the parallel arrangement of the $[C_3N_6H_7]^+$ groups almost along the diagonal of the unit cell. The small difference between n_x, n_y, and n_z leads to modest birefringence value.[72] $(C_3N_6H_7)_2SiF_6\cdot H_2O$ has a high density of $[C_3N_6H_7]^+$ groups, large band gaps and parallel $[C_3N_6H_7]^+$ groups, but the highly symmetric $[SiF_6]^{2-}$ octahedron is detrimental to optical anisotropy.[67] The birefringence of the crystal is relatively reduced when the $[C_3N_6H_7]^+$ groups are not uniformly arranged parallelly. For example, when the $[C_3N_6H_7]^+$ density of the $2(C_3N_6H_7)^+\cdot 2Cl^-\cdot H_2O$ crystal is 5.58 × 10^{-3} Å^{-3}, but the $[C_3N_6H_7]^+$ groups are not aligned parallelly, the birefringence is 0.28@546 nm.[53] The $[C_3N_6H_8]^{2+}$ units in the $(C_3H_8N_6)PbBr_4$ crystal are not uniformly oriented, and the density of $[C_3N_6H_8]^{2+}$ units is only 3.14 × 10^{-3} Å^{-3}. However, it still has a high birefringence (0.294 at 550 nm) due to the presence of Pb with a lone pair of electrons.[56] It is interesting to note that the $[C_3N_6H_7]^+$ groups in all four melamine-based compounds of the NCS structure are non-coplanar and parallel. There are several conclusions to be drawn from the analysis of the above points: (1) the density of $[C_3N_6H_7]^+$ groups can be effectively reduced and the coplanar arrangement of $[C_3N_6H_7]^+$ groups can be induced by introducing non-π-conjugated polyhedral units into the crystal structure. (2) The parallel coplanar arrangement of $[C_3N_6H_7]^+$ groups is more significant in enhancing crystal birefringence when comparing the effects of the $[C_3N_6H_7]^+$ group arrangement and its density on birefringence. (3) The introduction of a distorted polyhedral structure with a heavy metal as the center and a chlorine atom as the ligand, which is more favorable to breaking the dipole–dipole interaction of organic molecules and obtaining the NCS structure of the compound.

2.2 Optical crystals with $[C(NH_2)_3]^+$ cations

In this section, a number of compounds containing $[C(NH_2)_3]^+$ cations with excellent optical properties are presented. The band gap, UV cut-off edge, birefringence and SHG properties are summarized in Table 2. Some compounds with excellent properties are selected for discussion. It is found that the compounds with planar π-conjugated $[C(NH_2)_3]^+$ cations conjugated to non-π-conjugated tetrahedral units not only have more suitable birefringence, but also shorter UV cut-off edges. Owing to the synergistic effect of the nonlinear optically active units and the birefringent active groups, the SHG response and the birefringence of the nonlinear optical crystals are in balance.

$C(NH_2)_3BF_4$ crystallizes in the NCS space group $R3m$.[76] The planar π-conjugated $[C(NH_2)_3]^+$ units extend on the ab plane (Fig. 13a). The $[C(NH_2)_3]^+$ units are connected with the interlaced $[BF_4]^-$ units by hydrogen bonding to form a two-dimensional layer, which is stacked along the c direction. As shown

Table 2 Main optical properties of the compounds containing the $[C(NH_2)_3]^+$ cation

Number	Compound	Space group	Band gap[a] (eV)	Birefringence[b]	UV cut-off (nm)	SHG response[a]	Ref.
1	$[C(NH_2)_3]_3C_3N_3S_3$	*Fdd*2	3.05	0.076@550 nm	340	2 × KDP	77
2	$[C(NH_2)_3]_2Bi(NO_3)_3Cl_2$	$P2_1/c$	3.25	0.176@546 nm	365	—	78
3	$[C(NH_2)_3]_3V_2O_4F_5$	*C*2/*c*	3.29	0.35@546 nm	377	—	79
4	$[C(NH_2)_3]_6Mo_7O_{24}$	*Fdd*2	3.31	0.200@550 nm	313	1.3 × KDP	80
5	$C(NH_2)_3MoO_3(IO_3)$	*Cmca*	3.33	0.415@546 nm	330	—	81
6	$[C(NH_2)_3]_3Bi_2NO_3Cl_8$	$P\bar{1}$	3.33	0.166@546 nm	350	—	78
7	$C(NH_2)_3(HC_4O_4)$	$P2_1/c$	3.35	0.351@546 nm	370	—	82
8	$[C(NH_2)_3]_{10}(MoO_3)_{10}(PO_4)_2(HPO_4)_2{\cdot}5H_2O$	$P2_1/c$	3.43	0.203@550 nm	316	—	83
9	$C(NH_2)_3Rb(I_3O_8)(IO_3)(I_2O_6H_2)$	$P\bar{1}$	3.54	0.286@1064 nm	—	—	84
10	$[C(NH_2)_2NHNO_2][C(NH_2)_3](NO_3)_2$	*Cc*	3.58	0.090@550 nm	298	1.5 × KDP	85
11	$C(NH_2)_3Cd(C_2O_4)Cl(H_2O){\cdot}H_2O$	$P\bar{1}$	3.76	0.08@532 nm	—	—	86
12	$[C(NH_2)_3]BiCl_2SO_4$	$P\bar{1}$	3.85	0.12@546 nm	322	—	87
13	$C(NH_2)_3(I_3O_8)(HI_3O_8)(H_2I_2O_6)(HIO_3)_4{\cdot}3H_2O$	*P*1	3.89	0.06@550 nm	308	2.1 × KDP	88
14	$[C(NH_2)_3]_2MoO_2F_4{\cdot}H_2O$	*Imm*2	4	—	265	2.1 × KDP	89
15	$[C(NH_2)_3]Sb(C_2O_4)F_2{\cdot}H_2O$	$P2_1/c$	4.09	0.339@546 nm	303	—	90
16	$[C(NH_2)_3]_3VO_4{\cdot}2H_2O$	*Cc*	4.16	0.068@1064 nm	285	2.2 × KDP	91
17	$[C(NH_2)_3]_3PO_4{\cdot}2H_2O$	$Pna2_1$	4.2	0.055@546 nm[a]	250	1.5 × KDP	92
18	$[C(NH_2)_3]_2S_2O_8$	$P4_12_12$	4.25	0.102@546 nm	222	—	93
19	$(C(NH_2)_3)_2(I_2O_5F)(IO_3)(H_2O)$	$P2_1/c$	4.49	0.074@1064 nm	246	—	94
20	$[C(NH_2)_3]CF_3COO$	*Pbcn*	4.54[b]	0.085@532 nm	205	—	64
21	$[C(NH_2)_3]_3IO_3$	$P2_1/n$	4.57	0.070@1064 nm	242	—	94
22	$[C(NH_2)_3]HC_2O_4{\cdot}H_2O$	$P2_1/c$	4.66[b]	0.371@532 nm	254	—	64
23	$(C(NH_2)_3)[Er(HCOO)_4]$	$P2_12_12_1$	4.76	0.066@546 nm[a]	260	0.2 × KDP	95
24	$C(NH_2)_3SbF_4$	$P2_12_12_1$	4.8	0.08@532 nm	241	2 × KDP	96
25	$[C(NH_2)_3]SbFPO_4{\cdot}H_2O$	$P2_1/c$	4.8	0.14@546 nm	258	—	97
26	$[C(NH_2)_3]IO_2F_2$	$P\bar{1}$	4.81	0.121@1064 nm	230	—	94
27	$[C(NH_2)_3]_2SO_3S$	$P6_3mc$	4.88	0.121@1064 nm	254	2.8 × KDP	98
28	$C(NH_2)_3Sb_2F_7$	*Pbca*	4.9	0.055@532 nm	236	—	96
29	$[C(NH_2)_3]Br$	*Pnma*	5.07[b]	0.075@532 nm	206	—	64
30	$[C(NH_2)_3]_3(H_2C_3N_3O_3)_3(H_3C_3N_3O_3)$	$P\bar{1}$	5.08	0.402@400 nm	—	—	99
31	$[C(NH_2)_3]_2Sb_3F_3(HPO_3)_4$	*C*2/*c*	5.1	0.03@546 nm	243	—	97
32	$[C(NH_2)_3](H_2C_3N_3O_3)$	$P\bar{1}$	5.2	0.419@400 nm	—	—	99
33	$[C(NH_2)_3]_2(PF_6){\cdot}F$	*C*2/*c*	5.35[b]	0.072@532 nm	204	—	64
34	$[C(NH_2)_3]Al(SO_4)_2{\cdot}6H_2O$	*P*31*m*	5.36[b]	0.098@546 nm	<200	—	100
35	$C(NH_2)_3ClO_4$	*R*3*m*	5.43[b]	0.076@1064 nm	200	3 × KDP	101
36	$[C(NH_2)_3]PO_2H_2$	*Pnma*	5.44[b]	0.100@532 nm	201	—	64
37	$[C(NH_2)_3]_2[B_4O_5(OH)_4]{\cdot}2H_2O$	$P\bar{1}$	5.72	0.089@1064 nm	<200	—	102
38	$[C(NH_2)_3][B(C_2O_2H_4)_2]$	$Pna2_1$	5.76	0.080@550 nm	215	0.7 × KDP	103
39	$[C(NH_2)_3]_2Zn(CO_3)_2$	$P4_12_12$	5.9	—	210	0.5 × KDP	104
40	$[C(NH_2)_3]_3AsO_4{\cdot}2H_2O$	*Cc*	5.9	0.0405@546 nm	210	0.9 × KDP	105
41	$C(NH_2)_3B_5O_6(OH)_4{\cdot}H_2O$	$P\bar{1}$	5.91	0.094@1064 nm	197	—	102
42	$[C(NH_2)_3][CH_3PO_3H]$	*C*2/*m*	6.04[b]	0.114@1064 nm	195	—	106
43	$[C(NH_2)_3]_2[B_4O_5(OH)_4]{\cdot}H_2O$	$P\bar{1}$	6.05	0.099@1064 nm	194	—	102
44	$[C(NH_2)_3]_6(PO_4)_2{\cdot}3H_2O$	*Cc*	6.05	0.077@546 nm	205	3.8 × KDP	63
45	$Rb[C(NH_2)_3][B_4O_5(OH)_4]{\cdot}1.5H_2O$	*P*1	6.1	0.080@1064 nm	<190	0.2 × KDP	107
46	$C(NH_2)_3BF_4$	*R*3*m*	6.09[b]	0.12@546 nm[a]	193	4.03 × KDP	76
47	$(C(NH_2)_3)_2Zn(HPO_3)_2$	*Fdd*2	6.18	0.030@1064 nm	194	1 × KDP	108
48	$C(NH_2)_3SO_3F$	*R*3*m*	6.2	0.133@1064 nm	200	5 × KDP	65
49	$C(NH_2)_3SO_3CH_3$	*C*2/*m*	6.34[b]	0.137@1064 nm	195	—	109
50	$[C(NH_2)_3]_2[B_3O_3F_4(OH)]$	*P*1	6.36	0.161@1064 nm	195	1.4 × KDP	62
51	$[C(NH_2)_3][B_3O_3F_2(OH)_2]$	*P*1	6.53	0.173@1064 nm	190	0.9 × KDP	62
52	$K[C(NH_2)_3][B_4O_5(OH)_4]{\cdot}3H_2O$	$P\bar{1}$	6.65[b]	0.084@1064 nm	—	—	107
53	$[C(NH_2)_3]_2PO_3F$	*Cm*	6.55[b]	0.039@532 nm	194	1 × KDP	110
54	$(NH_4)[C(NH_2)_3][B_3O_3F_4(OH)]$	*C*2/*c*	6.69[b]	0.101@1064 nm	195	—	111
55	$C(NH_2)_3SO_3CF_3$	*C*2/*c*	6.81[b]	0.139@1064 nm	182	—	109
56	$C(NH_2)_3H_2PO_4$	$P2_1/c$	—	0.127@546 nm[a]	220	—	66
57	$[C(NH_2)_3]_2HPO_4{\cdot}H_2O$	$P\bar{4}2_1c$	—	0.0195@300 nm	220	0.59 × KDP	66
58	$[C(NH_2)_3]_3PO_4{\cdot}3/2H_2O$	*Cc*	—	—	—	0.23 × KDP	66
59	$[C(NH_2)_3]H_2PO_3$	$P2_1$	—	—	219	0.41 × KDP	112
60	$[C(NH_2)_3]HSeO_3$	$P2_1$	—	—	266	0.18 × KDP	112

[a] The experimental value. [b] The theoretical calculation value.

in Fig. 13b, the transparent crystals of $C(NH_2)_3BF_4$ with a size up to 40 × 30 × 21 mm^3 were grown using the solution cooling method. The $C(NH_2)_3BF_4$ crystal exhibits excellent linear and nonlinear optical properties, such as a short UV cutoff edge (193 nm), a large SHG coefficient (d_{eff} = 1.42 pm V^{-1}), a short phase matching wavelength (193.2 nm) and a high laser

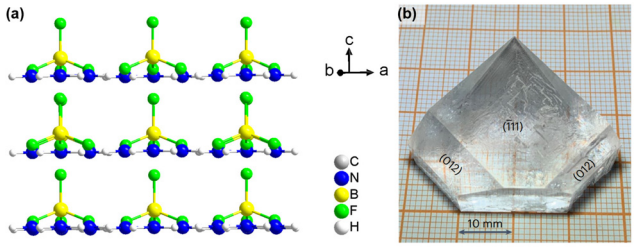

Fig. 13 (a) Crystal structure of $C(NH_2)_3BF_4$. (b) The as-grown crystal of $C(NH_2)_3BF_4$. Copyright 2023, The Author(s), under exclusive licence to Springer Nature Limited.

damage threshold. It is a promising nonlinear optical crystal material. In addition, the direct SHG output capability of the crystal in the whole transmission range is studied by means of the multistage frequency conversion scheme or optical parameter technique scheme. Based on the phase matching device, a 193.2–266 nm UV/deep UV tunable laser output has been achieved, which verifies that the crystal has full-wavelength phase-matching capability. The $C(NH_2)_3BF_4$ crystal is the first and only example of a UV/deep UV NLO crystal that has realized full-wavelength phase-matching.

$[C(NH_2)_3][B_3O_3F_2(OH)_2]$ belongs to the NCS space group $P1$.[62] As can be seen in Fig. 14, the basic unit of $[C(NH_2)_3][B_3O_3F_2(OH)_2]$ consists of the $[C(NH_2)_3]^+$ unit and $[B_3O_3F_2(OH)_2]^-$ groups. The $[B_3O_3F_2(OH)_2]^-$ group is connected with the $[C(NH_2)_3]^+$ cation by hydrogen bonds to form the 2D $\{[C(NH_2)_3][B_3O_3F_2(OH)_2]\}_\infty$ layer. The arrangement of $[C(NH_2)_3]^+$ cations and $[B_3O_3F_2(OH)_2]^-$ groups in the plane are constrained by the interaction of N–H···F, N–H···O and O–H···F hydrogen bonds in the layer. The interlayer hydrogen bond interactions can lead to the stacking of layers in a defined direction, forming the three-dimensional structure. $[C(NH_2)_3][B_3O_3F_2(OH)_2]$ exhibits a short UV cut-off edge of 190 nm, a large birefringence of 0.173@1064 nm, and an SHG response of 0.9 × KDP. Its optical properties are mainly derived from the ordered arrangement of planar $[C(NH_2)_3]^+$ units and $[B_3O_3F_2(OH)_2]^-$ groups. The hydrogen bonds between the $[C(NH_2)_3]^+$ units and $[B_3O_3F_2(OH)_2]^-$ groups align all the groups in almost the same direction, which is advantageous for enhancing the macroscopic SHG response and birefringence.

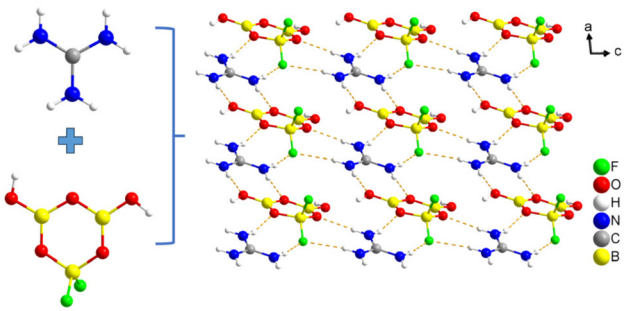

Fig. 14 Crystal structure of $[C(NH_2)_3][B_3O_3F_2(OH)_2]$.

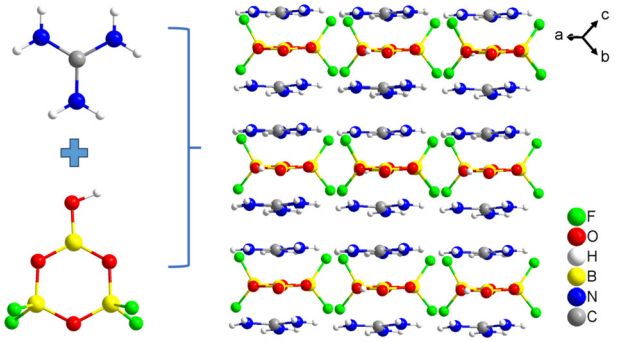

Fig. 15 Crystal structure of $[C(NH_2)_3][B_3O_3F_2(OH)_2]$.

In addition, a centimetre-sized crystal with good linear and nonlinear optical properties was obtained, which has broad application prospects in the deep ultraviolet region.

$[C(NH_2)_3]_2[B_3O_3F_4(OH)]$ crystallizes in the NCS space group $P1$.[62] As shown in Fig. 15, similar to the structure of $[C(NH_2)_3][B_3O_3F_2(OH)_2]$, the $[B_3O_3F_4(OH)]^{2-}$ unit is connected to the planar $[C(NH_2)_3]^+$ cation *via* hydrogen bonds to form the 2D $\{[C(NH_2)_3][B_3O_3F_4(OH)][C(NH_2)_3]\}_\infty$ layer. The layers are stacked by hydrogen bond interactions to form a three-dimensional structure. Optical measurements show that $[C(NH_2)_3]_2[B_3O_3F_4(OH)]$ not only exhibits a large SHG response (1.4 × KDP), but also has a short UV cutoff edge (195 nm) and a birefringence of 0.161@1064 nm. The optimal arrangement of coplanar $[C(NH_2)_3]^+$ cations and $[B_3O_3F_4(OH)]^{2-}$ groups endows the crystals with sufficient nonlinear optical coefficients, large birefringence values and wide band gaps. It has been demonstrated that $[C(NH_2)_3]_2[B_3O_3F_4(OH)]$ shows great potential as an NLO crystal.

$C(NH_2)_3SO_3F$ crystallizes in the NCS space group $R3m$.[65] The asymmetric unit consists of planar triangular $[C(NH_2)_3]^+$ units and a distorted $[SO_3F]^-$ tetrahedron (Fig. 16). The $[C(NH_2)_3]^+$ units and $[SO_3F]^-$ units are connected by N–H···O hydrogen bonds to form a two-dimensional honeycomb layer

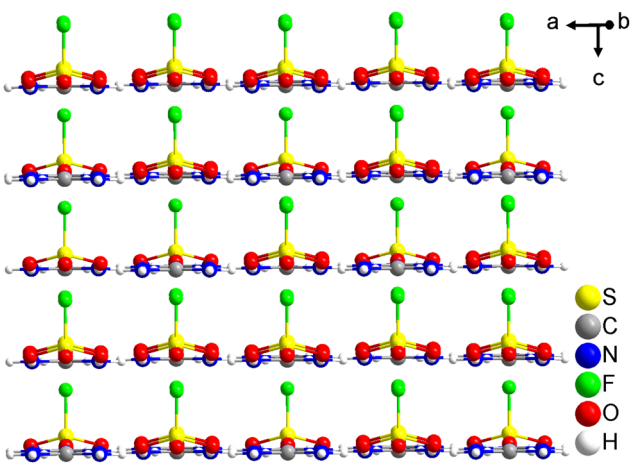

Fig. 16 Crystal structure of $C(NH_2)_3SO_3F$.

of $[C(NH_2)_3SO_3F]_\infty$. The $[C(NH_2)_3SO_3F]_\infty$ layers are stacked along the *c*-axis. The $[C(NH_2)_3SO_3F]_\infty$ layer is similar to the $[Be_2BO_3F_2]_\infty$ layer of KBBF. It can be considered that in the $[Be_2BO_3F_2]_\infty$ layer of KBBF, the planar $[BO_3]^{3-}$ units are replaced by the $[C(NH_2)_3]^+$ cations, and the BeO_3F tetrahedron is replaced by the SO_3F tetrahedron. All SO_3F tetrahedra are uniformly arranged within the $[C(NH_2)_3SO_3F]_\infty$ layer, which is conducive to enhancing the SHG response. $C(NH_2)_3SO_3F$ exhibits a short UV cutoff edge (200 nm), a strong SHG response (5 × KDP), and a large birefringence (0.133@1064 nm). The superior optical properties of $C(NH_2)_3SO_3F$ are primarily attributed to the coplanar configuration of $[C(NH_2)_3]^+$ units. The calculation shows that the $C(NH_2)_3SO_3F$ crystal is a promising ultraviolet nonlinear optical crystal with the shortest matching wavelength of 200 nm.

$[C(NH_2)_3]_2PO_3F$ crystallizes in the NCS space group *Cm*.[110] As shown in Fig. 17, the isolated planar π-conjugated $[C(NH_2)_3]^+$ cations are linked to the $[PO_3F]^-$ tetrahedral units *via* O–H···O hydrogen bonds to form a 3D structure. The $[C(NH_2)_3]_2PO_3F$ exhibits a short UV cut-off edge (194 nm) and a birefringence of 0.039@532 nm. Powder SHG measurements showed the SHG response (1.0 × KDP) of $[C(NH_2)_3]_2PO_3F$. The laser damage threshold is 91.5 mW cm^{-2}, which is 2.3 times higher than that of KDP (39.8 mW cm^{-2}). The PO_3F unit creates new routes for designing and selecting high-performance deep ultraviolet (DUV) NLO materials.

$[C(NH_2)_3]_3PO_4{\cdot}2H_2O$ belongs to the NCS orthorhombic space group $Pna2_1$.[92] As shown in Fig. 18a, all $[C(NH_2)_3]^+$ cation units are tilted towards the *c*-axis in approximately the same direction, which contributes positively to the NLO susceptibility. All $[PO_4]^{3-}$ tetrahedron units are fairly neatly aligned along the *c*-axis. However, the $[PO_4]^{3-}$ tetrahedra and the $[C(NH_2)_3]^+$ units are aligned almost opposite to each other along the *c*-direction, resulting in the cancellation of the portion of the SHG contribution from the $[C(NH_2)_3]^+$ units. The $[C(NH_2)_3]^+$ units and PO_4^{3-} units are connected through hydrogen bonds to form a three-dimensional network in the structure. $[C(NH_2)_3]_3PO_4{\cdot}2H_2O$ shows a significant SHG response (1.5 × KDP) and a short UV cut-off edge (250 nm). The experimental value of birefringence is 0.055@546 nm. The large birefringence mainly originates from the contribution of the planar $[C(NH_2)_3]^+$ cation units. Theoretical calculations

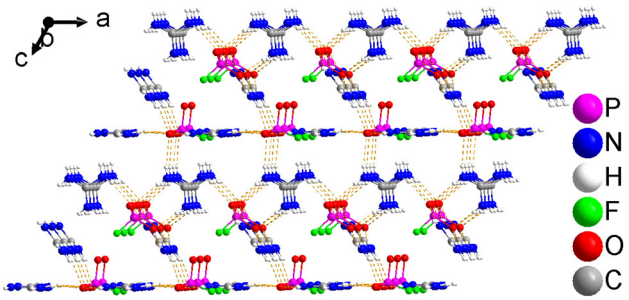

Fig. 17 Crystal structure of $C(NH_2)_3PO_3F$.

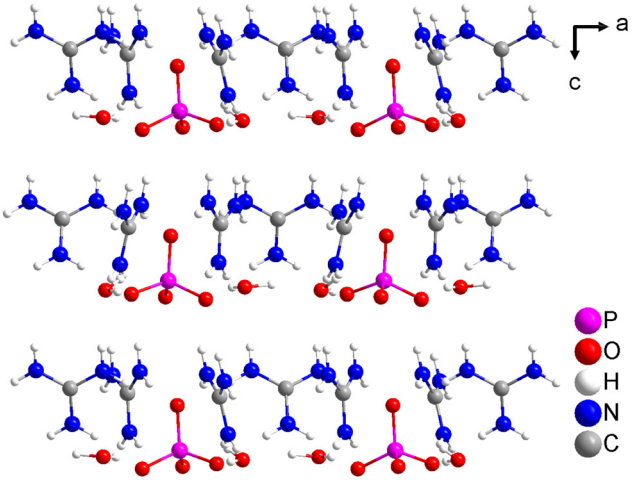

Fig. 18 Crystal structure of $[C(NH_2)_3]_3PO_4{\cdot}2H_2O$.

show that the excellent optical properties are mainly due to the synergistic effect of π-conjugated triangular planar $[C(NH_2)_3]^+$ units and non-π-conjugated tetrahedral $[PO_4]^{3-}$ units. The introduction of organic π-conjugated $[C(NH_2)_3]^+$ units into phosphates would be a feasible route for the synthesis of UV nonlinear optical phosphates with a large birefringence and SHG response.

$[C(NH_2)_3]_6(PO_4)_2{\cdot}3H_2O$ crystallizes in the NCS monoclinic space group *Cc*.[63] The planar triangle $[C(NH_2)_3]^+$ units, $[PO_4]^{3-}$ tetrahedra, and H_2O are interconnected by N–H···O and O–H···O hydrogen bonds to form a pseudo three-dimensional structure (Fig. 19). The cationic $[C(NH_2)_3]^+$ units exhibit large hyperpolarizability and optical anisotropy. The uniform arrangement of the $[PO_4]^{3-}$ units along the *c*-axis is favourable for a large SHG response and sufficient birefringence. $[C(NH_2)_3]_6(PO_4)_2{\cdot}3H_2O$ exhibits excellent optical properties, including a short UV cut-off edge (205 nm) and a high SHG response (3.8 × KDP at 1064 nm, 0.3 × β-BBO at 532 nm). The

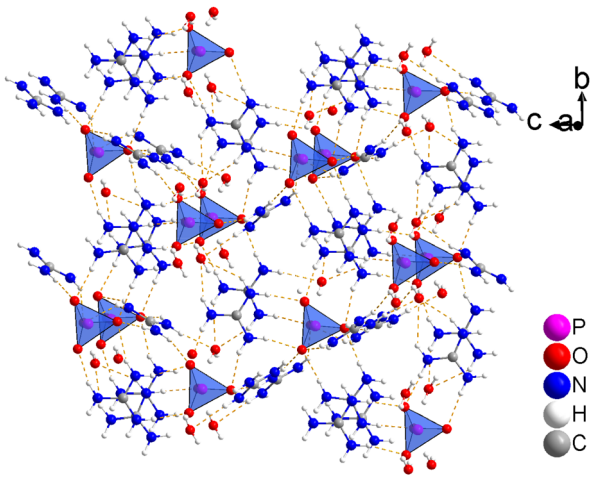

Fig. 19 Crystal structure of $[C(NH_2)_3]_6(PO_4)_2{\cdot}3H_2O$.

experimental birefringence is 0.078@546 nm (Δn_{cal} = 0.077@546 nm), and the short phase-matching SHG wavelength is 250 nm. Theoretical calculations show that the remarkable linear and nonlinear optical properties of $[C(NH_2)_3]_6(PO_4)_2{\cdot}3H_2O$ are mainly contributed by the synergistic effect of cationic $[C(NH_2)_3]^+$ planar triangles and anionic $[PO_4]^{3-}$ tetrahedra.

$C(NH_2)_3ClO_4$ belongs to the NCS space group $R3m$.[101] As shown in Fig. 20a, the planar $[C(NH_2)_3]^+$ units are arranged parallelly on the *ab* plane. The $[ClO_4]^-$ tetrahedron units are connected to the $[C(NH_2)_3]^+$ units by N–H···O hydrogen bonds to form a 2D $[C(NH_2)_3ClO_4]_\infty$ layer. All parallel $[C(NH_2)_3]^+$ planar triangular units are aligned in the same direction within the same layer, favouring a strong macroscopic SHG response and high optical anisotropy. It is interesting to note that all $[ClO_4]^-$ tetrahedra are also oriented in the same direction, which contributes to an enhanced SHG response. Centimetre-scale crystals of $C(NH_2)_3ClO_4$ were successfully grown using the solution method (Fig. 20b). $C(NH_2)_3ClO_4$ exhibits a short UV cut-off edge (200 nm), a moderate birefringence (0.076@1064 nm), and a large SHG response (3.0 × KDP). The calculated results show that the shortest SHG phase matching wavelength of $C(NH_2)_3ClO_4$ crystals is about 216 nm using the direct birefringent phase matching technique.

$[C(NH_2)_3][B(C_2O_2H_4)_2]$ belongs to the orthorhombic space group $Pna2_1$.[103] The structure is shown in Fig. 21. Its asymmetric unit contains $[C(NH_2)_3]^+$ units and the $[B(C_2O_2H_4)_2]^-$ anion group. It is interesting to note that the twisted '8'-shaped $[B(C_2O_2H_4)_2]^-$ anionic group is formed by the BO_4 tetrahedron sharing O atoms with two glycol molecules. The $[B(C_2O_2H_4)_2]^-$ groups are interlinked with the $[C(NH_2)_3]^+$ units by hydrogen bonds to form one-dimensional $[C(NH_2)_3][B(C_2O_2H_4)_2]_\infty$ chains. These chains are connected to each other in different directions by hydrogen bonds, forming two-dimensional $\{[C(NH_2)_3][B(C_2O_2H_4)_2]\}_\infty$ layers. The layers are interconnected through hydrogen bonds to form a three-dimensional network structure. $[C(NH_2)_3][B(C_2O_2H_4)_2]$ exhibits a short UV cutoff edge (215 nm) and a suitable birefringence (0.08@550 nm). The SHG response is about 0.7 × KDP. Theoretical calculations show that the optical properties are mainly contributed by the synergistic interaction between the $[B(C_2O_2H_4)_2]^-$ groups and $[C(NH_2)_3]^+$ units.

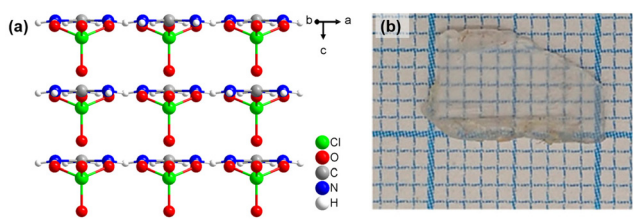

Fig. 20 (a) Crystal structure of $C(NH_2)_3ClO_4$. (b) The as-grown crystal of $C(NH_2)_3ClO_4$. Copyright 2021 The Authors. Published by American Chemical Society.

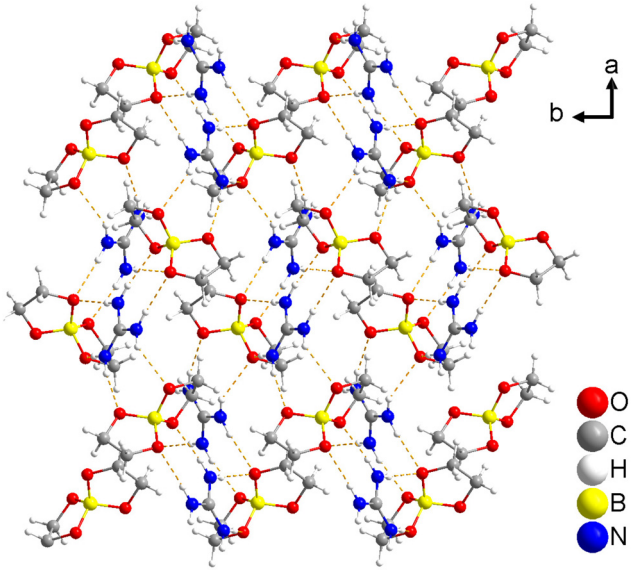

Fig. 21 Crystal structure of $[C(NH_2)_3][B(C_2O_2H_4)_2]$.

2.3 Optical crystals with other organic planar groups

In this section, several optical crystals containing $[C_5N_2H_7]^+$, $[C_5NOH_{5+x}]^{x+}$ (x = 0–1), $[C_4N_3H_6]^+$, $[C_4N_3OH_6]^+$, and $[C_3N_2H_5]^+$ groups with excellent properties are presented. The $[C_5N_2H_7]^+$, $[C_5NOH_{5+x}]^{x+}$ (x = 0–1), $[C_4N_3H_6]^+$ and $[C_4N_3OH_6]^+$ groups and planar π-conjugated organic cations with B_3O_6-type structures, exhibit high hyperpolarizabilities and large polarizability anisotropy, which serve as excellent optically active units and can be used to construct optical crystals with outstanding performance. The optical properties of the compounds are listed in Table 3.

$(C_5H_6ON)^+(H_2PO_4)^-$ crystallizes in the orthorhombic chiral NCS space group $P2_12_12_1$.[57] $(C_5H_6ON)^+(H_2PO_4)^-$ consists of a positively charged organic 4-hydroxypyridine $[C_5H_6ON]^+$ cation and a negatively charged inorganic dihydrogen phosphate $[H_2PO_4]^-$ anion. As shown in Fig. 22, the $[C_5H_6ON]^+$ and $[H_2PO_4]^-$ anions form alternating 'intercalation' structures through positive and negative electrostatic coulombic interactions and strong hydrogen-bond interactions. $[C_5H_6ON]^+$ groups are arranged by π–π stacking along the *a*-direction. The $[C_5H_6ON]^+$ cations are interconnected with $[H_2PO_4]^-$ anions by hydrogen bonds to form a strong hydrogen bond network. $(C_5H_6ON)^+(H_2PO_4)^-$ exhibits a wide transmission range (0.26–1.50 μm), a strong SHG response (3 × KDP), a large birefringence (Δn_{cal} = 0.25@1064 nm), and a high laser damage threshold (2.2 × KDP). The theoretical calculations show that the large optical anisotropy of $(C_5H_6ON)^+(H_2PO_4)^-$ is mainly contributed by the π-conjugated organic $[C_5H_6ON]^+$ cations, while the strong SHG response originates from the synergistic action of the distorted inorganic $[H_2PO_4]^-$ anions and the polar organic $[C_5H_6ON]^+$ cations. This work proposes the application of the "salt" strategy in eliminating dipole–dipole interactions using hydrogen bonds in order to avoid the centrosymmetric trap resulting from the polarity-induced suscepti-

Table 3 Main optical properties of the compounds containing the $[C_5H_6ON]^+$ or $[C_4H_6N_3]^+$ etc. cation

Number	Compound	Space group	Band gap[a] (eV)	Birefringence[b]	UV cut-off (nm)	SHG response[a]	Ref.
1	$(C_5H_7N_2)(Sb_2F_7)$	*Pn*	4.51	0.134@546 nm[a]	275	2 × KDP	59
2	$(o\text{-}C_5H_5NO)_2ZnCl_2$	*C*2/*c*	4.29	0.466@546 nm	275	—	114
3	$(C_5H_5NO)(Sb_2OF_4)$	*Cm*	4.59	0.513@546 nm[a]	270	12 × KDP	59
4	$[o\text{-}C_5H_6NO]_2[ZnCl_4]$	*C*2/*c*	4.52	0.193@546 nm	261	—	114
5	$(C_5H_6ON)^+(H_2PO_4)^-$	$P2_12_12_1$	4.69	0.25@1064 nm	264	3 × KDP	57
6	$(C_5H_6ON)^+(CH_3SO_3)^-$ (RTP)	$Pna2_1$	4.64	0.20@546 nm	252	3.3 × KDP	113
7	$(C_5H_6ON)_2[Sb_2O(C_2O_4)_3]$	*C*2/*c*	3.76	0.264@546 nm	270	—	115
8	$(C_4H_6N_3)^+(H_2PO_3)^-$	$P2_1$	3.27	0.225@589.3 nm[a]	346	2 × KDP	58
9	$C_4N_3H_6SO_3NH_2$	*Cm*	2.90	0.220@546 nm	350	2.5 × KDP	116
10	$(C_4H_6N_3O)(HSO_4)$	*Cc*	3.85	0.47@1064 nm	277	1.65 × KDP	60
11	$(C_3N_2H_5)B_3O_3F_2(OH)_2$	$P\bar{1}$	5.79	0.205@546 nm	214	—	117
12	$[C_3N_2H_5]_2C_2O_4{\cdot}H_2O$	*Pnna*	4.42	0.119@546 nm[a]	256	—	118
13	$[C_3N_2H_5]HC_2O_4$	$P2_1/n$	4.3	0.037@546 nm[a]	258	—	118
14	$(C_3N_2H_5)B_5O_6(OH)_4$	$P2_1/c$	5.27	0.107@1064 nm	<200	—	102
15	$(C_2N_3H_4)_2PbCl_4$ (300k)	*Cmcm*	3.4	0.17@550 nm	365	—	61

[a] The experimental value. [b] The theoretical calculation value.

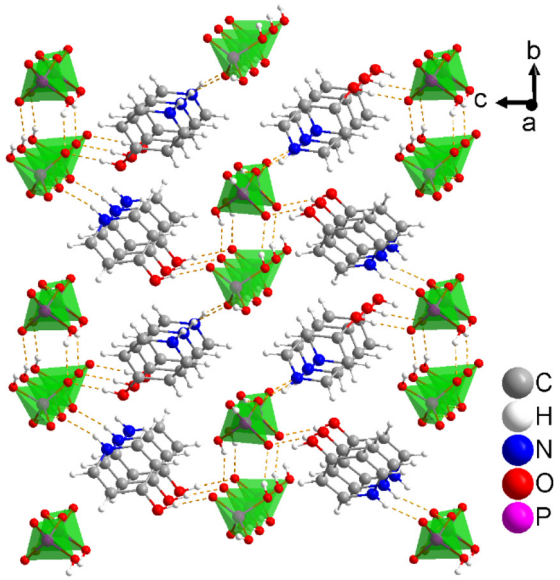

Fig. 22 Crystal structure of $(C_5H_6ON)^+(H_2PO_4)^-$.

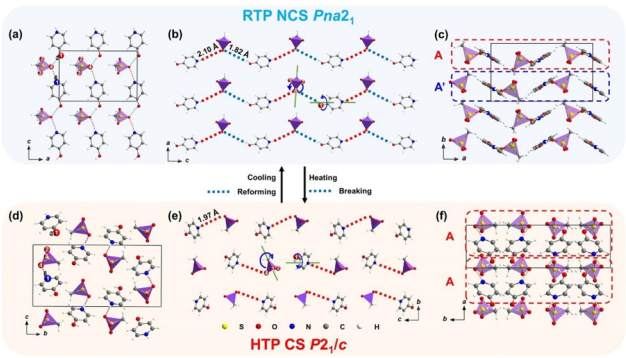

Fig. 23 Crystal structure of $(C_5H_6ON)^+(CH_3SO_3)^-$. Copyright 2024 Wiley.

bility. It shows a new way for rationally designing semi-organic materials with high optical properties in NCS structures.

The novel nonlinear optical switch $(C_5H_6ON)^+(CH_3SO_3)^-$(4HPMS) is a near-room-temperature thermally driven material. 4HPMS-RTP belongs to the NCS orthorhombic space group $Pna2_1$.[113] The $[CH_3SO_3]^-$ anion is connected with the $[C_5H_6ON]^+$ cation to form a one-dimensional chain extending along the *c*-axis direction (Fig. 23a and b). These chains are uniformly arranged along the *a*-axis direction to form pseudo two-dimensional layers. These layers are arranged in the -AA′ AA′- style (Fig. 23c). At 73 °C, due to thermal breaking of partial intermolecular hydrogen bonds, $(C_5H_6ON)^+(CH_3SO_3)^-$ undergoes rotation, and 4HPMS transforms from the NCS $Pna2_1$ room-temperature phase into the CS $P2_1/c$ phase. The zero-dimensional dimer structure in 4HPMS-HTP is retained in the *bc* plane, forming the pseudo-2D layer (Fig. 23d). These pseudo-layers are stacked along the *a*-axis in an -AAAA- pattern (Fig. 23f). $(C_5H_6ON)^+(CH_3SO_3)^-$ has excellent NLO switching properties, including a strong SHG response (3.3 × KDP), good cycling performance (>5 cycles), and a high laser damage threshold (2.5 × KDP). Theoretical calculations show that the band gap is determined by $[C_5H_6ON]^+$ and $[CH_3SO_3]^-$ groups, while the SHG response and birefringence are mainly contributed by $[C_5H_6ON]^+$ groups. The role of hydrogen bonds in the heat-driven NLO switch will provide useful insights into other materials with hydrogen bonds.

$(C_4H_6N_3)^+(H_2PO_3)^-$ crystallizes in the monoclinic chiral space group $P2_1$.[58] As shown in Fig. 24a, the $[H_2PO_3]^-$ tetrahedron is extended along the *c*-axis by hydrogen bonds (O–H···O) to form chains. The $[C_4H_6N_3]^+$ rings are connected to these chains by anionic–cationic hydrogen bonds to form a layer structure. The anion–cation hydrogen bonds bind the $[C_4H_6N_3]^+$ groups to form a uniform orientation in the monolayer. The strong intermolecular π-conjugated interaction between the $[C_4H_6N_3]^+$ rings is broken by the $[H_2PO_3]^-$ anion. The elimination of the strong dipole interaction between the $[C_4H_6N_3]^+$ molecules leads to the formation of NCS structures of $(C_4H_6N_3)^+(H_2PO_3)^-$. The crystals of $(C_4H_6N_3)^+(H_2PO_3)$ with

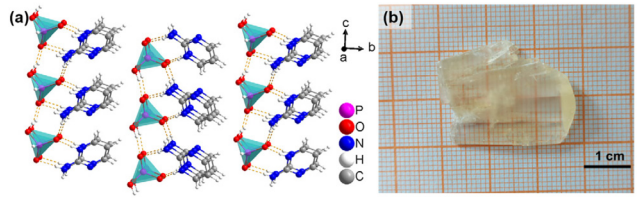

Fig. 24 (a) Crystal structure of $(C_4H_6N_3)^+(H_2PO_3)^-$. (b) The as-grown crystal of $(C_4H_6N_3)^+(H_2PO_3)$. Copyright 2022 American Chemical Society.

a size of 28 × 22 × 4 mm^3 were grown from the aqueous solution (Fig. 24b). $(C_4H_6N_3)^+(H_2PO_3)^-$ exhibits good nonlinear/linear optical properties, including a strong SHG response with phase matching behavior (2 × KDP), a large birefringence (0.225@589.3 nm), and a high LIDT (1.7 × KDP). Theoretical calculations show that the synergistic effect of $[C_4H_6N_3]^+$ groups and $[H_2PO_3]^-$ units determines the band gap, while the SHG response and birefringence are mainly contributed by the organic $[C_4H_6N_3]^+$ groups in a coplanar arrangement.

$C_4N_3H_6SO_3NH_2$ belongs to the monoclinic NCS space group *Cm*.[116] As shown in Fig. 25, all $[C_4N_3H_6]^+$ groups are arranged parallelly in the same direction in the *bc* plane. The planar arrangement structure contributes positively to the macroscopic optical anisotropy. All $[NH_2SO_3]^-$ units are also arranged parallelly in the same direction in the *b* direction. In the *bc* plane, the $[C_4N_3H_6]^+$ groups are connected to the $[NH_2SO_3]^-$ units by hydrogen bonds to form a 2D layer. Meanwhile, the hydrogen bonds formed between the anions and cations fix the position of the $[NH_2SO_3]^-$ units between the layers. In the *b* direction, the S–N bonds of the $[NH_2SO_3]^-$ units act as bridges connecting the layers consisting of $[C_4N_3H_6]^+$ groups to form a 3D network structure. $C_4N_3H_6SO_3NH_2$ exhibits a strong SHG response (2.5 × KDP) and a large birefringence (0.22@546 nm). Theoretical calculation analysis shows that the strong SHG response and large optical anisotropy originate from the parallel arrangement of planar π-conjugated $[C_4N_3H_6]^+$ groups.

$(C_5H_5NO)(Sb_2OF_4)$ crystallizes in the polar monoclinic NCS space group *Cm* (no. 8).[59] The *cis*-$[Sb_2O_2F_4]$ dimers are bonded to the neutral $[C_5H_5NO]$ groups *via* a shared O atom to form mirror-symmetric polar $[(C_5H_5NO)(Sb_2OF_4)]$ building blocks (Fig. 26a). Polar $[(C_5H_5NO)(Sb_2OF_4)]$ building blocks are interconnected by hydrogen bonds (N–H···O) to form one-dimensional chains (Fig. 26b). The one-dimensional chains are connected to each other along the *c*-axis by intermolecular forces (Fig. 26c). $(C_5H_7N_2)(Sb_2F_7)$ crystallizes in the polar monoclinic NCS space group *Pn* (no. 7).[59] Two $[SbF_4]^-$ seesaw-like polyhedra are connected to form a quasi-rigid polar *trans*-$[Sb_2F_7]^-$ dimer (Fig. 26d). The positively charged cation $[C_5H_7N_2]^+$ and the negatively charged dimer $[Sb_2F_7]^-$ are connected by hydrogen bonds to form 2D layers (Fig. 26e). The 2D layers are stacked in the -AAA- style along the *a*-axis (Fig. 26f). $(C_5H_5NO)(Sb_2OF_4)$ and $(C_5H_7N_2)(Sb_2F_7)$ exhibit excellent linear and nonlinear optical properties, including a strong SHG response (12 × KDP/2 × KDP), a large birefringence (0.513@546 nm/0.134@546 nm) and a short UV cut-off edge (270 nm/275 nm). Theoretical studies and structural analyses show that the polarised ionic bond interactions in the $(C_5H_5NO)(Sb_2OF_4)$ structure facilitate the proper alignment of the organic and inorganic groups and significantly improve the optical nonlinearity. This work elucidates for the first time that bonding interactions have an important role in the nonlinear optical properties of materials.

$(C_2N_3H_4)_2PbCl_4$ is a two-dimensional layered organic–inorganic hybrid halide perovskite crystal with thermotropic phase transition.[61] Its calculated birefringence decreases from 0.17@550 nm to 0.14@550 nm when the temperature is increased from 300 K to 380 K. The energy dispersive X-ray (EDX) spectroscopy mapping analysis illustrates the presence and uniform distribution of the elements Pb, Cl, C and N in the $(C_2N_3H_4)_2PbCl_4$ single crystal (Fig. 27a). $(C_2N_3H_4)_2PbCl_4$ crystallizes in the orthorhombic space group *Cmcm* (no. 63) at 300 K. The basic structural units of $(C_2N_3H_4)_2PbCl_4$ are the $PbCl_6$ octahedron and the $[C_2N_3H_4]^+$ groups. As shown in

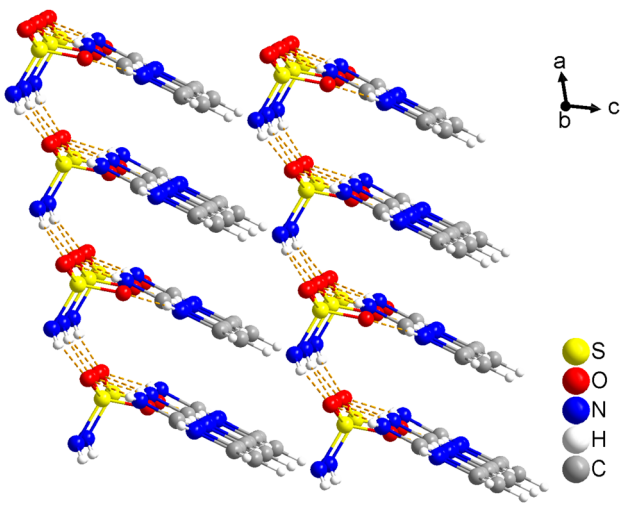

Fig. 25 Crystal structure of $C_4N_3H_6SO_3NH_2$.

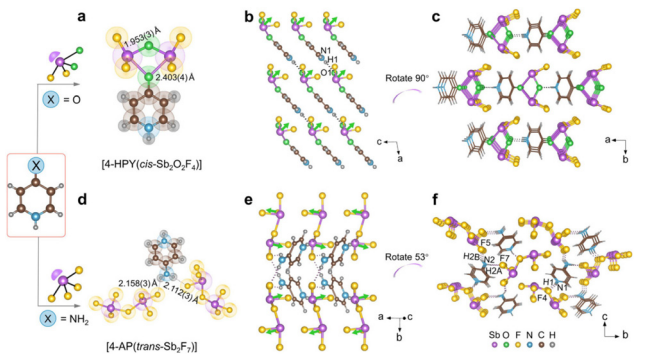

Fig. 26 Crystal structure of $(C_5H_5NO)(Sb_2OF_4)$ and $(C_5H_7N_2)(Sb_2F_7)$. Copyright 2024 American Chemical Society.

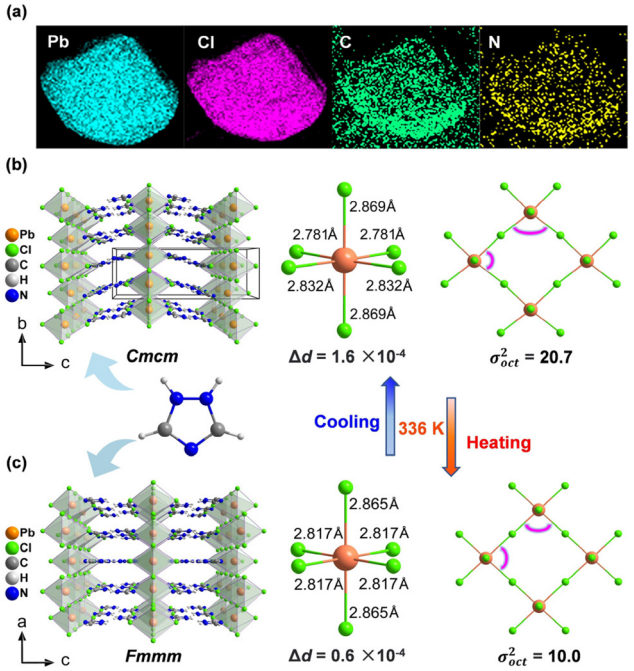

Fig. 27 (a) EDX mapping of $(C_2N_3H_4)_2PbCl_4$. (b) Crystal structure of $(C_2N_3H_4)_2PbCl_4$ at 300 K. (c) Crystal structure of $(C_2N_3H_4)_2PbCl_4$ at 380 K. Copyright 2023 Wiley.

Fig. 27b, the $PbCl_6$ octahedra form perovskite two-dimensional layers by corner sharing. The inorganic layer of the $PbCl_6$ octahedra is inserted into two sets of $[C_2N_3H_4]^+$ layers parallel to each other. The octahedral elongation (Δd) and octahedral angle variance $\sigma_{oct}{}^2$ of the $PbCl_6$ octahedra are 1.6×10^{-4} and 20.7, respectively, which indicate that the $PbCl_6$ octahedra have a high degree of distortion. When the temperature reaches 380 K, $(C_2N_3H_4)_2PbCl_4$ transitions from the orthorhombic space group *Cmcm* to *Fmmm*. All the $[C_2N_3H_4]^+$ groups are coplanar in the *bc* plane. The octahedral elongation (Δd) and octahedral angle variance $\sigma_{oct}{}^2$ of the $PbCl_6$ octahedra are 0.6×10^{-4} and 10, respectively, indicating that the distortion degree of the $PbCl_6$ octahedron decreased. Theoretical calculation analyses indicate that the planar π-conjugated $[C_2N_3H_4]^+$ groups and the $PbCl_6$ octahedron contribute to the birefringence and that the decrease in the distortion degree of the $PbCl_6$ octahedron after the phase transition is responsible for the heat switching birefringence.

3. Conclusion

In summary, this paper retrospects the progress in the research of optical crystals of planar π-conjugated organic cationic groups containing C=N bonds ($[C_3N_6H_7]^+$, $[C(NH_2)_3]^+$, $[C_5NOH_6]^+$ and $[C_4N_3H_6]^+$ groups). Their crystal structures and optical properties (including cut-off edge, birefringence and SHG response) are described in detail while highlighting the relationship among their rich and diverse chemical compositions, flexible structures and optical properties. Based on the classification, summary and analysis in this review, the following conclusions can be made:

1. Except for $C_3H_8N_6I_6{\cdot}3H_2O$, the compounds with $[C_3N_6H_{6+x}]^{x+}$ (x = 0–2) groups have birefringence in the range of 0.093@1064 nm to 0.44@546 nm, with the short cut-off edges ranging from 206 to 374 nm, located in the UV spectral region. The compounds with $[C_3N_6H_7]^+$ groups have a higher chance of exhibiting a large birefringence by modulating the parallel arrangement of the melamine rings.

2. The compounds containing the $[C(NH_2)_3]^+$ cation exhibit birefringence varying widely in the range of 0.0195@300 nm to 0.415@546 nm. The cut-off edge is located in the UV/DUV spectral region. The compounds containing the $[C(NH_2)_3]^+$ cation are more likely to be transmissive in the DUV spectral region than the compounds with $[C_3N_6H_7]^+$ or $[C_5NOH_6]^+$ and $[C_4N_3H_6]^+$ groups, that is to say, the compounds containing the $[C(NH_2)_3]^+$ cation are more likely to be used as DUV optical crystal materials. For nonlinear optical properties, the compounds with the $[C(NH_2)_3]^+$ cation in the NCS structure are more likely to achieve shorter phase-matching wavelengths. In the structure of $C(NH_2)_3SO_3F$, planar π-conjugated $[C(NH_2)_3]^+$ cations and isolated $[SO_3F]^-$ units are arranged in a uniform parallel manner. It is therefore concluded that $C(NH_2)_3SO_3F$ has excellent nonlinear and linear optical properties.

3. The compounds with $[C_5N_2H_7]^+$, $[C_5NOH_{5+x}]^{x+}$ (x = 0–1), $[C_4N_3H_6]^+$, $[C_4N_3OH_6]^+$, and $[C_3N_2H_5]^+$ groups have large birefringence values ranging from 0.037@546 nm to 0.513@546 nm with cut-off edges in the DUV/UV spectral region. It is noteworthy that the compounds are synthesized using $[C_5NOH_6]^+$ or $[C_4N_3H_6]^+$ groups in combination with tetrahedral units, which may break the dipole–dipole interactions between organic cations, avoiding the centrosymmetric traps and forming NCS structures.

The relationship between the crystal structure and optical properties has been extensively and intensively studied. It is noteworthy that compounds containing organic conjugated ring molecules tend to crystallise in the CS space group. One reason is that the stacking efficiency of organic conjugated ring molecules is higher in the CS structure than that in the NCS structure; another reason is that the organic groups have large dipole moments, and they can easily reach antiparallel arrangements because the dipole–dipole interactions between the molecules drive the crystallisation of these molecules in a CS arrangement. It is well known that the symmetry of a crystal depends to a large extent on the type, arrangement and layout of the groups. More importantly, electronegative elements, non-π-conjugated polyhedra, metallic elements and their coordination geometries also have a significant impact on the symmetry of crystals. The purposeful construction of NLO crystal materials with planar π-conjugated organic cationic groups containing C=N bonds that have excellent optical properties by rationally designing and assembling optically active groups is becoming an attractive research topic. Therefore, subsequent research work should place emphasis on the following points:

1. The introduction of halogens and d^0 and d^{10} atoms into melamine-based compounds is favourable for the formation of

distorted tetrahedra centred on heavy metal ions to obtain NCS structures. However, the introduction of d^0 and d^{10} atoms may cause a red shift in the cutoff edge of the compounds. In consideration of the important role of melamine in increasing optical anisotropy, it can be used as a potential gene for designing birefringent materials.

2. The selection of conjugated small molecular $[C(NH_2)_3]^+$ units as cations can effectively improve the transmission range of the crystals towards shorter wavelengths. The six coplanar hydrogen atoms of the $[C(NH_2)_3]^+$ unit can form hydrogen bonds with atoms of high electronegativity (N/O/F). Intramolecular hydrogen bonds are not only favourable to the growth habit of crystals, but also to the thermal stability and mechanical properties of crystals. When $[C(NH_2)_3]^+$ units are integrated with non-π-conjugated tetrahedral units, the tetrahedral units can modulate the planar arrangement of $[C(NH_2)_3]^+$ units, which provides more possibilities to explore excellent UV/DUV nonlinear optical materials.

3. The combination of organic ring groups with highly electronegative atoms (such as halogens, O and N) can easily form hydrogen bonds in the crystal structure, which is expected to eliminate the original dipole–dipole effect and promote the formation of NCS structure crystals with excellent optical properties.

This paper provides a comprehensive review of the current research progress in the structure and optical properties of crystal materials containing cationic organic planar π-conjugated groups with C=N bonds. Additionally, it offers an outlook on future developments in this field. It is anticipated that this paper will serve as a valuable reference for researchers seeking to explore high-performance optical crystal materials within semi-organic systems.

Data availability

The authors confirm that the data supporting the findings of this study are available within the article and its ESI.

Conflicts of interest

There are no conflicts to declare.

Acknowledgements

This work was supported by the National Natural Science Foundation of China (22335007 and 22361132544) and the Xinjiang Major Science and Technology Project (2021A01001).

References

1 D. Cyranoski, Materials science: China's crystal cache, *Nature*, 2009, **457**, 953.
2 W. J. Yao, R. He, X. Y. Wang, Z. S. Lin and C. T. Chen, Analysis of deep-uv nonlinear optical borates: approaching the end, *Adv. Opt. Mater.*, 2014, **2**, 411.
3 W. B. Zhang, X. L. Hou, S. J. Han and S. L. Pan, Toward the ultraviolet (UV) or deep-UV nonlinear optical crystals: the combination of π-conjugated planar $[XY_3]$ and tetrahedral $[XY_4]$, *Coord. Chem. Rev.*, 2024, **505**, 215664.
4 M. F. Wu, E. Tikhonov, A. Tudi, I. Kruglov, X. Hou, C. Xie, S. L. Pan and Z. H. Yang, Target-driven design of deep-ultraviolet nonlinear optical materials via interpretable machine learning, *Adv. Mater.*, 2023, **35**, 2300848.
5 P. S. Halasyamani and J. M. Rondinelli, The must-have and nice-to-have experimental and computational requirements for functional frequency doubling deep-uv crystals, *Nat. Commun.*, 2018, **9**, 2972.
6 K. M. Ok, E. O. Chi and P. S. Halasyamani, Bulk characterization methods for non-centrosymmetric materials: second-harmonic generation, piezoelectricity, pyroelectricity, and ferroelectricity, *Chem. Soc. Rev.*, 2006, **35**, 710.
7 C. T. Chen, T. Sasaki, R. K. Li, Y. C. Wu, Z. S. Lin, Y. Mori, Z. G. Hu, J. Y. Wang, G. Aka and M. Yoshimura, *Nonlinear optical borate crystals: Principals and applications*, John Wiley & Sons, 2012.
8 W. B. Cai, A. Abudurusuli, C. W. Xie, E. Tikhonov, J. J. Li, S. L. Pan and Z. H. Yang, Toward the rational design of mid-infrared nonlinear optical materials with targeted properties via a multi-level data-driven approach, *Adv. Funct. Mater.*, 2022, **32**, 2200231.
9 M. Zhang, D. H. An, C. Hu, X. L. Chen, Z. H. Yang and S. L. Pan, Rational design via synergistic combination leads to an outstanding deep-ultraviolet birefringent $Li_2Na_2B_2O_5$ material with an unvalued B_2O_5 functional gene, *J. Am. Chem. Soc.*, 2019, **141**, 3258.
10 M. Mutailipu, K. R. Poeppelmeier and S. L. Pan, Borates: a rich source for optical materials, *Chem. Rev.*, 2020, **121**, 1130.
11 A. Tudi, S. J. Han, Z. H. Yang and S. L. Pan, Potential optical functional crystals with large birefringence: recent advances and future prospects, *Coord. Chem. Rev.*, 2022, **459**, 214380.
12 J. D. Bierlein and H. Vanherzeele, Potassium titanyl phosphate: properties and new applications, *J. Opt. Soc. Am. B*, 1989, **6**, 622.
13 C. T. Chen, B. C. Wu, A. D. Jiang and G. M. You, A new-type ultraviolet shg crystal beta-bab_2o_4, *Sci. Sin., Ser. B*, 1985, **28**, 235.
14 C. T. Chen, Y. C. Wu, A. D. Jiang, B. C. Wu, G. M. You, R. K. Li and S. J. Lin, New nonlinear optical crystal: LiB_3O_5, *J. Opt. Soc. Am. B*, 1989, **6**, 616–621.
15 Y. Mori, I. Kuroda, S. Nakajima, T. Sasaki and S. Nakai, New nonlinear optical crystal: Cesium lithium borate, *Appl. Phys. Lett.*, 1995, **67**, 1818.
16 B. B. Zhang, G. Q. Shi, Z. H. Yang, F. F. Zhang and S. L. Pan, Fluorooxoborates: beryllium–free deep–ultraviolet nonlinear optical materials without layered growth, *Angew. Chem., Int. Ed.*, 2017, **56**, 3916.

17 C. T. Chen, G. L. Wang, X. Y. Wang and Z. Y. Xu, Deep-UV nonlinear optical crystal $KBe_2BO_3F_2$—discovery, growth, optical properties and applications, *Appl. Phys. B*, 2009, **97**, 9.
18 M. J. Bloemer and M. Scalora, Transmissive properties of Ag/MgF_2 photonic band gaps, *Appl. Phys. Lett.*, 1998, **72**, 1676.
19 G. Q. Zhou, J. Xu, X. D. Chen, H. Y. Zhong, S. T. Wang, K. Xu, P. Z. Deng and F. X. Gan, Growth and spectrum of a novel birefringent α-BaB_2O_4 crystal, *J. Cryst. Growth*, 1998, **191**, 517.
20 G. Ghosh, Dispersion-equation coefficients for the refractive index and birefringence of calcite and quartz crystals, *Opt. Commun.*, 1999, **163**, 95.
21 M. Mutailipu, M. Zhang, H. P. Wu, Z. Yang, Y. H. Shen, J. L. Sun and S. L. Pan, $Ba_3Mg_3(BO_3)_3F_3$ polymorphs with reversiblep phase transition and high performances as nonlinear optical materials, *Nat. Commun.*, 2018, **9**, 3089.
22 F. F. Zhang, X. L. Chen, M. Zhang, W. Q. Jin, S. J. Han, Z. H. Yang and S. L. Pan, An excellent deep-ltraviolet birefringent material based on $[BO_2]_\infty$ infinite chains, *Light: Sci. Appl.*, 2022, **11**, 252.
23 B. H. Lei, S. L. Pan, Z. H. Yang, C. Cao and D. J. Singh, Second harmonic generation susceptibilities from symmetry adapted wannier functions, *Phys. Rev. Lett.*, 2020, **125**, 187402.
24 Z. T. Yan, J. B. Fan, S. L. Pan and M. Zhang, Recent advances in rational structure design for nonlinear optical crystals: leveraging advantageous templates, *Chem. Soc. Rev.*, 2024, **53**, 6568.
25 Y. Zhou, Z. F. Guo, H. G. Gu, Y. Q. Li, Y. P. Song, S. Y. Liu, M. C. Hong, S. G. Zhao and J. H. Luo, A solution-processable natural crystal with giant optical anisotropy for efficient manipulation of light polarization, *Nat. Photonics*, 2024, 1.
26 C. T. Chen, Y. C. Wu and R. K. Li, The anionic group theory of the non-linear optical effect and its applications in the development of new high-quality nlo crystals in the borate series, *Int. Rev. Phys. Chem.*, 1989, **8**, 65.
27 N. Ye, Q. X. Chen, B. C. Wu and C. T. Chen, Searching for new nonlinear optical materials on the basis of the anionic group theory, *J. Appl. Phys.*, 1998, **84**, 555.
28 S. J. Han, A. Tudi, W. B. Zhang, X. L. Hou, Z. H. Yang and S. L. Pan, Recent development of Sn^{II}, Sb^{III}-based birefringent material: crystal chemistry and investigation of birefringence, *Angew. Chem., Int. Ed.*, 2023, **62**, e202302025.
29 C. M. Huang, M. Mutailipu, F. F. Zhang, C. Hu, Z. H. Yang, L. Y. Wang, X. Zhou, K. R. Poeppelmeier and S. L. Pan, Pushing the limits of borates with functionalized $[BO_2]^-$ units, *Nat. Commun.*, 2021, **12**, 2597.
30 L. Xiong, L. M. Wu and L. Chen, A general principle for duv nlo materials: π-conjugated confinement enlarges band gap, *Angew. Chem.*, 2021, **133**, 25267.
31 G. Q. Shi, Y. Wang, F. F. Zhang, B. B. Zhang, Z. H. Yang, X. L. Hou, S. L. Pan and K. R. Poeppelmeier, Finding the next deep-ultraviolet nonlinear optical material: $NH_4B_4O_6F$, *J. Am. Chem. Soc.*, 2017, **139**, 10645.
32 X. F. Wang, Y. Wang, B. B. Zhang, F. F. Zhang, Z. H. Yang and S. L. Pan, CsB_4O_6F: a congruent–melting deep–ultraviolet nonlinear optical material by combining superior functional units, *Angew. Chem., Int. Ed.*, 2017, **56**, 14119.
33 Y. Wang, B. B. Zhang, Z. H. Yang and S. L. Pan, Cation-tuned synthesis of fluorooxoborates: towards optimal deep-ultraviolet nonlinear optical materials, *Angew. Chem., Int. Ed.*, 2018, **57**, 2150.
34 B. B. Zhang, G. P. Han, Y. Wang, X. L. Chen, Z. H. Yang and S. L. Pan, Expanding frontiers of ultraviolet nonlinear optical materials with fluorophosphates, *Chem. Mater.*, 2018, **30**, 5397.
35 W. Q. Jin, W. Y. Zhang, A. Tudi, L. Y. Wang, X. Zhou, Z. H. Yang and S. L. Pan, Fluorine-driven enhancement of birefringence in the fluorooxosulfate: a deep evaluation from a joint experimental and computational study, *Adv. Sci.*, 2021, **8**, 2003594.
36 X. D. Zhang, L. C. Guo, B. B. Zhang, J. Yu, Y. Wang, K. Wu, H. J. Wang and M. H. Lee, From silicates to oxonitridosilicates: improving optical anisotropy for phase-matching as ultraviolet nonlinear optical materials, *Chem. Commun.*, 2021, **57**, 639.
37 M. Mutailipu, Z. H. Yang and S. L. Pan, Toward the enhancement of critical performance for deep-ultraviolet frequency-doubling crystals utilizing covalent tetrahedra, *Acc. Mater. Res.*, 2021, **2**, 282.
38 B. B. Zhang, E. Tikhonov, C. W. Xie, Z. H. Yang and S. L. Pan, Prediction of fluorooxoborates with colossal second harmonic generation (SHG) coefficients and extremely wide band gaps: towards modulating properties by tuning the BO_3/BO_3F ratio in layers, *Angew. Chem., Int. Ed.*, 2019, **58**, 11726.
39 B. L. Cheng, W. J. Ma, A. Tudi, F. F. Zhang, Z. L. Chen, X. L. Hou, Z. H. Yang and S. L. Pan, Fluorooxoborate promoting the exploration of short-wavelength linear and nonlinear optical crystals with expected properties and versatile structures, *Chem. Mater.*, 2023, **35**, 5671.
40 M. Mutailipu, F. M. Li, C. C. Jin, Z. H. Yang, K. R. Poeppelmeier and S. L. Pan, Strong nonlinearity induced by coaxial alignment of polar chain and dense $[BO_3]$ units in $CaZn_2(BO_3)_2$, *Angew. Chem., Int. Ed.*, 2022, **61**, e202202096.
41 G. H. Zou, N. Ye, L. Huang and X. S. Lin, Alkaline-alkaline earth fluoride carbonate crystals $ABCO_3F$ (A = K, Rb, Cs; B = Ca, Sr, Ba) as nonlinear optical materials, *J. Am. Chem. Soc.*, 2011, **133**, 20001.
42 M. Cheng, W. Q. Jin, Z. H. Yang and S. L. Pan, Large optical anisotropy-oriented construction of a carbonate-nitrate chloride compound as a potential ultraviolet birefringent material, *Chem. Sci.*, 2022, **13**, 13482.
43 Y. X. Song, M. Luo, C. S. Lin and N. Ye, Structural modulation of nitrate group with cations to affect shg responses in $RE(OH)_2NO_3$ (RE = La, Y, and Gd): new polar materials with large nlo effect after adjusting pH values of reaction systems, *Chem. Mater.*, 2017, **29**, 896.
44 X. H. Meng, X. Y. Zhang, Q. X. Liu, Z. Y. Zhou, X. X. Jiang, Y. G. Wang, Z. S. Lin and M. J. Xia, Perfectly encoding

π-conjugated anions in the $RE_5(C_3N_3O_3)(OH)_{12}$ (RE = Y, Yb, Lu) family with strong second harmonic generation response and balanced birefringence, *Angew. Chem., Int. Ed.*, 2023, **62**, e202214848.

45 J. Lu, Y. K. Lian, L. Xiong, Q. R. Wu, M. Zhao, K. X. Shi, L. Chen and L. M. Wu, How to maximize birefringence and nonlinearity of π-conjugated cyanurates, *J. Am. Chem. Soc.*, 2019, **141**, 16151.

46 D. H. Lin, M. Luo, C. S. Lin, F. Xu and N. Ye, KLi$(HC_3N_3O_3)\cdot 2H_2O$: Solvent-drop grinding method toward the hydro-isocyanurate nonlinear optical crystal, *J. Am. Chem. Soc.*, 2019, **141**, 3390.

47 D. H. Lin, M. Luo, C. S. Lin, L. L. Cao and N. Ye, An optimal arrangement of $(H_2C_4N_2O_3)^{2-}$ groups in the first non-centrosymmetric alkali barbiturate $Li_2(H_2C_4N_2O_3)\cdot 2H_2O$ inducing a giant second harmonic generation response and a striking birefringence, *Cryst. Growth Des.*, 2020, **20**, 4904.

48 Y. Y. Xu, C. S. Lin, D. H. Lin, M. Luo, D. Zhao, L. L. Cao and N. Ye, Explorations of second-order nonlinear optical materials in the alkaline earth barbiturate system: Noncentrosymmetric $Ca(H_3C_4N_2O_3)_2\cdot H_2O$ and centrosymmetric $Sr(H_5C_8N_4O_5)_2\cdot 4H_2O$, *Inorg. Chem.*, 2020, **59**, 15962.

49 L. L. Wu, H. X. Fan, C. S. Lin and M. Luo, Compounds consisting of coplanar π-conjugated B_3O_6-typed structures: an emerging source of ultraviolet nonlinear optical materials, *Chin. J. Struct. Chem.*, 2023, **42**, 100019.

50 F. Yang, L. Wang, Y. W. Ge, L. Huang, D. J. Gao, J. Bi and G. H. Zou, $K_4Sb(SO_4)_3Cl$: the first apatite-type sulfate ultraviolet nonlinear optical material with sharply enlarged birefringence, *J. Alloys Compd.*, 2020, **834**, 155154.

51 Y. Z. Huang, L.-M. Wu, X. T. Wu, L. H. Li, L. Chen and Y. F. Zhang, $Pb_2B_5O_9I$: an iodide borate with strong second harmonic generation, *J. Am. Chem. Soc.*, 2010, **132**, 12788.

52 K. C. Zhang and X. M. Wang, *Nonlinear Optical Crystal Materials Science*, Science Press, 2nd edn, 2005.

53 L. H. Liu, C. L. Hu, Z. Y. Bai, F. F. Yuan, Y. S. Huang, L. Z. Zhang and Z. B. Lin, $2(C_3H_7N_6)^+\cdot 2Cl^-\cdot H_2O$: an ultraviolet nonlinear optical crystal with large birefrigence and strong second-harmonic generation, *Chem. Commun.*, 2020, **56**, 14657.

54 L. H. Liu, Z. Y. Bai, L. Hu, D. S. Wei, Z. B. Lin and L. Z. Zhang, A melamine-based organic–inorganic hybrid material revealing excellent optical performance and moderate thermal stability, *J. Mater. Chem. C*, 2021, **9**, 7452.

55 C. C. Jin, F. M. Li, Z. H. Yang, S. L. Pan and M. Mutailipu, $[C_3N_6H_7]_2[B_3O_3F_4(OH)]$: a new hybrid birefringent crystal with strong optical anisotropy induced by mixed functional units, *J. Mater. Chem. C*, 2022, **10**, 6590.

56 W. Q. Huang, X. Zhang, Y. Q. Li, Y. Zhou, X. Chen, X. Q. Li, F. F. Wu, M. C. Hong, J. H. Luo and S. G. Zhao, A hybrid halide perovskite birefringent crystal, *Angew. Chem., Int. Ed.*, 2022, **61**, e202202746.

57 J. Lu, X. Liu, M. Zhao, X. B. Deng, K. X. Shi, Q. R. Wu, L. Chen and L. M. Wu, Discovery of nlo semiorganic $(C_5H_6ON)^+(H_2PO_4)^-$: dipole moment modulation and superior synergy in solar-blind UV region, *J. Am. Chem. Soc.*, 2021, **143**, 3647.

58 Z. P. Zhang, X. Liu, X. M. Liu, Z. W. Lu, X. Sui, B. Y. Zhen, Z. S. Lin, L. Chen and L. M. Wu, Driving nonlinear optical activity with dipolar 2-aminopyrimidinium cations in $(C_4H_6N_3)^+(H_2PO_3)^-$, *Chem. Mater.*, 2022, **34**, 1976.

59 L. Qi, X. X. Jiang, K. Duanmu, C. Wu, Z. S. Lin, Z. P. Huang, M. G. Humphrey and C. Zhang, Record second-harmonic generation and birefringence in an ultraviolet antimonate by bond engineering, *J. Am. Chem. Soc.*, 2024, **146**, 9975.

60 M. H. Lv, S. F. Li, J. Wang, J. X. Wang, R. L. Tang, H. B. Huang, B. B. Zhang and D. Yan, $(C_4H_6N_3O)(HSO_4)$: a cytosinium bisulfate with large birefringence and moderate second harmonic generation effect produced via combining a promising planar nonlinear optical-active motif with a tetrahedral group, *Inorg. Chem.*, 2024, **63**, 10943.

61 Z. Y. Wang, X. Chen, Y. P. Song, Z. P. Du, Y. Zhou, M. J. Li, W. Q. Huang, Q. T. Xu, Y. Q. Li, S. E. Zhao and J. H. Luo, A two-dimensional hybrid perovskite with heat switching birefringence, *Angew. Chem., Int. Ed.*, 2023, **62**, e202311086.

62 C. C. Jin, H. Zeng, F. Zhang, H. T. Qiu, Z. H. Yang, M. Mutailipu and S. L. Pan, Guanidinium fluorooxoborates as efficient metal-free short-wavelength nonlinear optical crystals, *Chem. Mater.*, 2021, **34**, 440.

63 C. Wu, X. X. Jiang, Z. J. Wang, H. Y. Sha, Z. S. Lin, Z. P. Huang, X. F. Long, M. G. Humphrey and C. Zhang, Uv solar-blind-region phase-matchable optical nonlinearity and anisotropy in a π-conjugated cation-containing phosphate, *Angew. Chem., Int. Ed.*, 2021, **60**, 14806.

64 M. Xia, M. Mutailipu, F. M. Li, Z. H. Yang and S. L. Pan, Finding short-wavelength birefringent crystals with large optical anisotropy activated by π-conjugated $[C(NH_2)_3]$ units, *Cryst. Growth Des.*, 2021, **21**, 1869.

65 M. Luo, C. S. Lin, D. H. Lin and N. Ye, Rational design of the metal-free $KBe_2BO_3F_2$·(KBBF) family member $C(NH_2)_3SO_3F$ with ultraviolet optical nonlinearity, *Angew. Chem., Int. Ed.*, 2020, **59**, 15978.

66 I. Němec, I. Matulková, P. Held, J. Kroupa, P. Němec, D. X. Li, L. Bohatý and P. Becker, Crystal growth, crystal structure, vibrational spectroscopy, linear and nonlinear optical properties of guanidinium phosphates, *Opt. Mater.*, 2017, **69**, 420.

67 Y. G. Shen, L. Ma, G. F. Dong, H. L. Yu and J. H. Luo, β-$(C_3H_7N_6)_2Cl_2\cdot H_2O$ and $C_3H_7N_6)F\cdot H_2O$: two UV birefringent crystals induced by uniformly aligned structural groups, *Inorg. Chem. Front.*, 2023, **10**, 2022.

68 D. Y. Dou, Q. Shi, Y. J. Bai, C. Chen, B. B. Zhang and Y. Wang, $C_3N_6H_7SO_3NH_2$: non-π-conjugated tetrahedra decoupling π-conjugated groups achieving large optical anisotropy and wide band gap, *Mater. Chem. Front.*, 2023, **7**, 5924.

69 H. W. Jia, D. Xu, Z. J. Li, M. Arif, Y. S. Jiang and X. L. Hou, $(C_3N_6H_7)BF_4{\cdot}H_2O$ and $(C_3N_6H_7)SO_3CH_3{\cdot}H_2O$ with large birefringence induced by coplanar π-conjugated $[C_3N_6H_7]^+$ groups, *Inorg. Chem. Front.*, 2024, DOI: **10.1039/D4QI01061B**.

70 W. Q. Huang, X. L. Wu, B. Ahmed, Y. Q. Li, Y. Zhou, H. Wang, Y. P. Song, X. J. Kuang, J. H. Luo and S. G. Zhao, A hybrid halide lead-free pseudo-perovskite with large birefringence, *Inorg. Chem. Front.*, 2023, **10**, 2039.

71 L. H. Liu, F. F. Yuan, Y. S. Huang, Z. B. Lin and L. Z. Zhang, Two uv optical crystals with strong optical anisotropy, large band gaps and an α-BBO type structure, *Dalton Trans.*, 2023, **52**, 5798.

72 Z. Y. Bai, J. Lee, H. Kim, C. L. Hu and K. M. Ok, Unveiling the superior optical properties of novel melamine-based nonlinear optical material with strong second-harmonic generation and giant optical anisotropy, *Small*, 2023, **19**, 2301756.

73 S. F. Li, L. Hu, Y. Ma, F. F. Mao, J. Zheng, X. D. Zhang and D. Yan, Noncentrosymmetric $(C_3H_7N_6)_6(H_2PO_4)_4(HPO_4){\cdot}4H_2O$ and centrosymmetric $(C_3H_7N_6)_2SO_4{\cdot}2H_2O$: Exploration of acentric structure by combining planar and tetrahedral motifs via hydrogen bonds, *Inorg. Chem.*, 2022, **61**, 10182.

74 Y. G. Shen, B. Chen, H. Chen and J. H. Luo, $(C_3N_6H_7)_2SbF_5{\cdot}H_2O$ exhibiting strong optical anisotropy from the optimal arrangement of π-conjugated $(C_3N_6H_7)^+$ groups, *Inorg. Chem.*, 2022, **61**, 14242.

75 Y. G. Shen, Y. W. Zhou, X. L. Xue, H. L. Yu, S. G. Zhao and J. H. Luo, $(C_3N_6H_7)_2SiF_6{\cdot}H_2O$: an ultraviolet birefringent crystal exceeding the intrinsic energy gap of an organic reagent, *Inorg. Chem. Front.*, 2022, **9**, 5226.

76 M. Mutailipu, J. Han, Z. Li, F. M. Li, J. J. Li, F. F. Zhang, X. F. Long, Z. H. Yang and S. L. Pan, Achieving the full-wavelength phase-matching for efficient nonlinear optical frequency conversion in $C(NH_2)_3BF_4$, *Nat. Photonics*, 2023, **17**, 694.

77 M. J. Li, Z. Y. Wang, B. Ahmed, Y. Q. Li, H. Wang, Y. P. Song, X. Y. Song, X. J. Kuang, J. H. Luo and S. G. Zhao, A second-order nonlinear optical material consisting of two π-conjugated groups, *ChemPlusChem*, 2023, **88**, e202300094.

78 Z. Y. Bai and K. M. Ok, Exceptional optical anisotropy enhancement achieved through dual-ions cosubstitution strategy in novel hybrid bismuth halides, *Small*, 2024, 2311391.

79 W. Y. Zhang, Z. C. Li, X. D. Leng, Q. Jing and Q. Wen, Enhancement of birefringence in π-conjugated oxyfluorides achieved via van der Waals layered structural optimization, *Cryst. Growth Des.*, 2024, **24**, 3140.

80 M. H. Lv, S. F. Li, M.-M. Ren, J. X. Wang, R. L. Tang, J. Chen, H. B. Huang, B. B. Zhang and D. Yan, $[C(NH_2)_3]_6Mo_7O_{24}$: a guanidinium molybdate as a UV nonlinear optical crystal with large birefringence, *Inorg. Chem.*, 2024, **63**, 3948.

81 W. Zeng, Y. Tian, X. H. Dong, L. Huang, H. M. Zeng, Z. Lin and G. H. Zou, $C(NH_2)_3MoO_3(IO_3)$: a molybdenyl iodate with giant birefringence designed via a cation–anion synergetic interaction strategy, *Chem. Mater.*, 2024, **36**, 2138.

82 H. M. Wang, Q. Wang, Q. Wang, L. L. Cao, L. Huang, D. J. Gao, J. Bi and G. H. Zou, Yin–yang complementarity strategy achieving giant optical anisotropy in a metal-free birefringent material $C(NH_2)_3(HC_4O_4)$, *Cryst. Growth Des.*, 2022, **22**, 4236.

83 Y. Zhang, M. H. Lv, S. F. Li, H. B. Huang, B. B. Zhang and D. Yan, $[C(NH_2)_3]_{10}(MoO_3)_{10}(PO_4)_2(HPO_4)_2{\cdot}5H_2O$: synergy effect of multiple functional units results in significant birefringence, *J. Solid State Chem.*, 2024, 124823.

84 D. Yan, Y. Ma, R. L. Tang, L. Hu, F. F. Mao, J. Zheng, X. D. Zhang and S. F. Li, $C(NH_2)_3Rb(I_3O_8)(IO_3)(I_2O_6H_2)$: an unprecedented organic–inorganic hybrid polyiodate with two different polyiodate groups, *J. Solid State Chem.*, 2022, **315**, 123530.

85 D. Yan, M. M. Ren, Q. Liu, F. F. Mao, Y. Ma, R. L. Tang, H. B. Huang, B. B. Zhang, X. D. Zhang and S. F. Li, $[C(NH_2)_2NHNO_2][C(NH_2)_3](NO_3)_2$: a mixed organic cationic hybrid nitrate with an unprecedented nonlinear-optical-active unit, *Inorg. Chem.*, 2023, **62**, 4757.

86 W. Xu, L. Ma, Y. L. Lv, S. Y. Ma, W. L. Liu, S. P. Guo and R. L. Tang, $C(NH_2)_3Cd(C_2O_4)Cl(H_2O){\cdot}H_2O$ and $BaCd(C_2O_4)_{1.5}Cl(H_2O)_2$: two oxalate chlorides obtained by chemical scissors strategy exhibiting low-dimensional structural networks and balanced overall optical properties, *Inorg. Chem.*, 2023, **63**, 67.

87 X. H. Dong, Z. Z. Zhang, L. Huang and G. H. Zou, $[C(NH_2)_3]BiCl_2SO_4$: an excellent birefringent material obtained by multifunctional group synergy, *Inorg. Chem. Front.*, 2022, **9**, 5572.

88 D. Yan, M. M. Ren, F. F. Mao, Y. Ma, R. L. Tang, B. B. Zhang, Y. Ma, X. D. Zhang and S. F. Li, $C(NH_2)_3(I_3O_8)(HI_3O_8)(H_2I_2O_6)(HIO_3)_4{\cdot}3H_2O$: an unprecedented asymmetric guanidinium polyiodate with a strong second-harmonic-generation response and a wide band gap, *Inorg. Chem.*, 2023, **62**, 1323.

89 W. Zeng, Y. Tian, L. Huang, H. M. Zeng, Z. E. Lin and G. H. Zou, $[C(NH_2)_3]_2MoO_2F_4{\cdot}H_2O$: unique chinese-knot structure revealing superior nonlinear-optical properties, *Inorg. Chem.*, 2022, **61**, 14523.

90 D. Zhang, Q. Wang, L. Y. Ren, L. L. Cao, L. Huang, D. J. Gao, J. Bi and G. H. Zou, Sharp enhancement of birefringence in antimony oxalates achieved by the cation–anion synergetic interaction strategy, *Inorg. Chem.*, 2022, **61**, 12481.

91 Z. Y. Bai, Y. Kuk, J. Lee, H. Kim and K. M. Ok, Guanidinium vanadate $[C(NH_2)_3]_3VO_4{\cdot}2H_2O$ revealing enhanced second-harmonic generation and wide band gaps, *Inorg. Chem.*, 2024, **63**, 3578.

92 X. Wen, C. S. Lin, M. Luo, H. X. Fan, K. C. Chen and N. Ye, $[C(NH_2)_3]_3PO_4{\cdot}2H_2O$: a new metal-free ultraviolet nonlinear optical phosphate with large birefringence and second-harmonic generation response, *Sci. China Mater.*, 2021, **64**, 2008.

93 M. Zhang, B. B. Zhang, D. Q. Yang and Y. Wang, $[C(NH_2)_3]_2S_2O_8$: combining delocalized and localized π-conjugate units to achieve strong optical anisotropy, *Inorg. Chem. Front.*, 2022, **9**, 6067.
94 J. H. Cui, S. B. Wang, A. Tudi, M. Q. Gai, Z. H. Yang and S. L. Pan, $(C(NH_2)_3)_2(I_2O_5F)(IO_3)(H_2O)$ and $C(NH_2)_3IO_2F_2$: two guanidine fluorooxoiodates with wide band gap and large birefringence, *Inorg. Chem.*, 2023, **63**, 661.
95 W. B. Liu, J. C. B. Jiang, C. Wu, Z. P. Huang and C. Zhang, A UV transparent rare earth metal formate exhibiting second harmonic generation response and moderate birefringence, *Chin. J. Inorg. Chem.*, 2024, **40**, 281.
96 M. Zhang, B. B. Zhang, D. Q. Yang and Y. Wang, Synergistic effect of π-conjugated $[C(NH_2)_3]$ cation and Sb(III) lone pair stereoactivity on structural transformation and second harmonic generation, *Inorg. Chem.*, 2021, **60**, 18483.
97 X. H. Dong, Y. Long, L. Huang, L. L. Cao, D. J. Gao, J. Bi and G. H. Zou, Large optical anisotropy differentiation induced by the anion-directed regulation of structures, *Inorg. Chem. Front.*, 2022, **9**, 6441.
98 Y. C. Liu, X. M. Liu, Z. Y. Xiong, B. W. Liu, J. L. Xu, L. N. Li, S. G. Zhao, Z. S. Lin, M. C. Hong and J. H. Luo, 2D van der Waals layered $[C(NH_2)_3]_2SO_3S$ exhibits desirable UV nonlinear-optical trade-off, *Inorg. Chem.*, 2021, **60**, 14544.
99 X. M. Liu, L. Kang, R. X. Guo and Z. S. Lin, Two metal-free cyanurate crystals with a large optical birefringence resulting from the combination of π-conjugated units, *Dalton Trans.*, 2021, **50**, 17495.
100 Y. R. Shang, H. Y. Sha, Z. J. Wang, R. B. Su, C. He, X. M. Yang and X. F. Long, The birefringence modulation in short-wave ultraviolet sulfates with functional π-conjugated cations and polymerized heteroleptic tetrahedral anions, *Adv. Opt. Mater.*, 2024, 2302844.
101 Y. X. Song, M. Luo, D. H. Lin, C. S. Lin, Z. J. Wang, X. F. Long and N. Ye, π-conjugated trigonal planar $[C(NH_2)_3]^+$ cationic group: a superior functional unit for ultraviolet nonlinear optical materials, *ACS Omega*, 2021, **6**, 9263.
102 C. H. Hu, M. F. Wu, M. Zhang, J. Han, X. L. Hou, F. Zhang, Z. H. Yang and S. L. Pan, "Cation activation": an effective strategy for the enhancement of birefringence, *Adv. Opt. Mater.*, 2023, **11**, 2300579.
103 J. X. Wang, S. F. Li, M. M. Ren, M. H. Lv, R. L. Tang, J. Chen, H. B. Huang, B. B. Zhang and D. Yan, $[C(NH_2)_3][B(C_2O_2H_4)_2]$: an organic–inorganic hybrid borate containing nonlinear-optical active unit $[B(C_2O_2H_4)_2]^-$ with solar-blind-region optical nonlinearity, *Inorg. Chem.*, 2024, **63**, 4487.
104 Z. Y. Bai, L. H. Liu, Z. B. Lin and K. M. Ok, $[C(NH_2)_3]_2Zn(CO_3)_2$: a guanidinium-templated ultraviolet nonlinear optical material, *Inorg. Chem.*, 2022, **61**, 12473.
105 D. M. Wang, Z. Z. Wei, Z. Y. Bai, L. H. Liu, Z. B. Lin and L. Z. Zhang, Hybrid organic–inorganic triguanidine arsenate dihydrate for ultraviolet nonlinear optical application, *Dalton Trans.*, 2022, **51**, 463.
106 H. T. Qiu, R. An, J. J. Li, Z. H. Yang, S. L. Pan and M. Mutailipu, Tetrahedra modification of phosphates for optical anisotropy enhancement, *Adv. Opt. Mater.*, 2024, DOI: 10.1002/adom.202401866.
107 Z. Q. Chen, C. Y. Liu, J. J. Li, Z. H. Yang, S. L. Pan and M. Mutailipu, Hydrogen bond-derived symmetry transformation in hydroxyborates: Converting the nonlinearity from null to active, *Mater. Today Chem.*, 2024, **40**, 102277.
108 J. J. Zhang, X. M. Zhang, Y. Wang, K. Wu and B. B. Zhang, Phosphites: a nonlinear optical materials system with a wide band gap and moderate second-harmonic generation effect, *Inorg. Chem.*, 2022, **61**, 18622.
109 H. Zhou, M. Cheng, D. D. Chu, X. Liu, R. An, S. L. Pan and Z. H. Yang, Sulfate derivatives with heteroleptic tetrahedra: new deep–ultraviolet birefringent materials in which weak interactions modulate functional module ordering, *Angew. Chem., Int. Ed.*, 2024, e202413680.
110 L. Xiong, J. Chen, J. Lu, C. Y. Pan and L. M. Wu, Monofluorophosphates: a new source of deep-ultraviolet nonlinear optical materials, *Chem. Mater.*, 2018, **30**, 7823.
111 Z. Q. Chen, F. M. Li, Z. H. Yang, S. L. Pan and M. Mutailipu, Hydroxyfluorooxoborate $(NH_4)[C(NH_2)_3][B_3O_3F_4(OH)]$ for exploring the effects of cation substitution on structure and optical properties, *Chem. Commun.*, 2023, **59**, 12435.
112 I. Němec, I. Matulková, W. Krumbe, L. Andersen, I. Císařová, J. Kroupa, P. Němec, L. Bohatý and P. Becker, Linear and nonlinear optical properties, pyroelectricity and vibrational spectroscopy of polar guanidinium hydrogen phosphite, GuH_2PO_3, and hydrogen selenite, $GuHSeO_3$, *Opt. Mater.*, 2021, **111**, 110722.
113 L. Chen, Z. P. Zhang, X. Liu, R. X. Wang, S. Zhao, W. J. He, H. Y. Chen, X. B. Deng, L. M. Wu and Z. Y. Zhou, Remarkable second harmonic generation response in $(C_5H_6NO)^+(CH_3SO_3)^-$: unraveling the role of hydrogen bond in thermal driven nonlinear optical switch, *Angew. Chem., Int. Ed.*, 2024, e202408551.
114 Y. Li and K. M. Ok, Breaking boundaries: Giant ultraviolet birefringence in dimension-reduced Zn-based crystals, *Angew. Chem., Int. Ed.*, 2024, DOI: 10.1002/anie.202409336.
115 D. X. Jiao, H. L. Zhang, C. He, S. Y. Chen, K. Wang, X. H. Zhang, L. Wei and Q. Wei, Layered $(C_5H_6ON)_2[Sb_2O(C_2O_4)_3]$ with a large birefringence derived from the uniform arrangement of π-conjugated units, *Chin. J. Struct. Chem.*, 2024, **43**, 100304.
116 D. Y. Dou, Q. Shi, H. M. Li, B. B. Zhang, D. Q. Yang and Y. Wang, Rational combination of π–conjugated and non–π–conjugated groups achieving strong nonlinear optical response, large optical anisotropy, and UV light–switchable fluorescence, *Adv. Sci.*, 2024, **11**, 2401325.
117 C. H. Hu, C. J. Shen, H. Zhou, J. Han, Z. H. Yang, K. R. Poeppelmeier, F. Zhang and S. L. Pan, $(C_3N_2H_5)B_3O_3F_2(OH)_2$: realizing large birefringence via a synergistic effect between anion F/OH–ratio optimization and cation activation, *Small Struct.*, 2024, 2400296.
118 C. H. Hu, J. J. Liu, J. L. Qu, J. H. Hu and X. Z. Jiang, Achieving great optical anisotropy with the well-directed alignment of π-conjugated groups due to hydrogen bonds, *J. Saudi Chem. Soc.*, 2024, **28**, 101789.

